Design, Electron Transfer Process, and Opto-Electronic Property of Solar Cell Using Triphenylamine-Based D-π-A Architectures

Yuanchao Li [1], Lu Mi [1], Haibin Wang [1], Yuanzuo Li [1],* and Jianping Liang [2],*

[1] College of Science, Northeast Forestry University, Harbin 150040, China; liyuanchao2018@126.com (Y.L.); milufine@sina.com (L.M.); whbhit@126.com (H.W.)

[2] Key Lab of Materials Modification, Ministry of Education, Dalian University of Technology, Dalian 116024, China

* Correspondence: yzli@nefu.edu.cn (Y.L.); liangjp0601@mail.dlut.edu.cn (J.L.); Tel.: +86-451-82192245-8211 (Y.L.)

check for updates

Abstract: A series of D-π-A type dyes were designed based on the experimentally synthesized A1 by introducing different functional groups on the donor and π-spacer, and the optical and electrical properties were calculated by using density functional theory (DFT) and time-dependent DFT (TD-DFT). P1–P6 present highest light harvesting efficiency (LHE), driving force of electron injection (ΔG^{inject}), reorganization energy (ΔG_{reg}) and eV_{OC}. These critical parameters have a close relationship with the short-circuit current density (J_{SC}) and open-circuit photovoltage (V_{OC}), and lead to P1–P6 will exhibit higher efficiency. D4 also exhibit superior properties in the driving force of electron injection (ΔG^{inject}), reorganization energy (ΔG_{reg}), which will lead to a higher short-circuit current density (J_{SC}). We hope that these results will be helpful for experiments to synthesize new and highly efficient dyes.

Keywords: opto-electronic property; dye-sensitized solar cells; density functional theory; electronic structure

1. Introduction

Efficient development and utilization of renewable energy is an important way to solve energy shortage. Solar energy has received wide attention compared with other renewable energy sources due to its unlimited supply. Since Grätzel and O'Regan reported dye-sensitized solar cells (DSSC) in 1991 [1], it is quickly regarded as an alternative to silicon solar cells because of their easy production processes and lower production prices [2–7]. Dye sensitizer is a key part of DSSC to improve performance, and a series of dyes have been studied including porphyrin dyes, Ru-based dyes (such as N3/N719 [8] and the black dyes [9]) and metal-free organic dyes. Ru-based dyes and porphyrin dyes are regarded as promising sensitizers, and the power conversion efficiency (PCE) have reached 13% [10]. However, it is not ideal for large-scale production due to high cost, not being environmentally friendly, and a complex synthesis and purification process [11,12]. Therefore, metal-free organic dyes have become an alternative to Ru-based dyes and porphyrin dyes for their high molar extinction coefficient, low cost, and ease of synthesis [13–17].

The literature reports many different structures organic sensitizers including D-A, D-π-A, D-π-A-π-D, D-D-π-A, D-A-π-A, and D-π-π-A [18–24]. Among them, the most metal-free organic dyes have donor-π-acceptor (D-π-A) structure [25], mainly including prophyrin dyes [26,27], coumarin dyes [28,29], triphenylamine dyes [30,31], indoline dyes [32,33], and so on. The D-π-A structure with acceptor (such as sulfonic acid, cyanoacrylic acid, phosphonic acid, and carboxylic acid) binds to the

semiconductor (TiO$_2$) surface, which will facilitate electron transfer to the TiO$_2$ and the regeneration of excited dyes to the ground state by the redox shuttle [14]. Metal-free organic dyes with D-π-A structure have been widely used in DSSC due to the above advantages [34,35]. Among reported D-π-A structure, triphenylamine and cyanoacrylic acid were regarded as excellent donor and acceptor units [36,37]. Previous research indicates that dye with D-π-A structure can efficiently promote intramolecular charge transfer from the donor to acceptor moiety, which will lead to broadening the absorption spectrum and increasing the charge carrier mobility [38,39]. In order to achieve high power conversion efficiency, the dyes should meet the following requirements [40], dyes should have enough driving force to effective electron injection, and the oxidation potential must be lower than that of redox potential of I^-/I_3^- electrolyte, which facilitates oxidation dye regeneration. There should be a strong electronic coupling between the dye acceptor and the semiconductor substrate, which ensures charge transfer channel perfect electron injection. The absorption spectrum should have a strong absorption in the region of 400–600 nm. Recently, Chen et al. [41] synthesized two novel dyes CC201 and CC202, they exhibit strong response in the region of 500−800 nm. CC202 exhibits higher power conversion efficiency (PCE) of 6.1% with cobalt electrolyte. Kim et al. [42] designed two D-π-A dyes IAH and IDH to study the effect of the alkyl chain location at different positions on the photoelectric properties. IAH exhibits more electron injection from the excited dye to the conduction band of TiO$_2$, which leads to a high short-circuit photocurrent (J_{SC}). IDH more effectively inhibits electron transfer from the TiO$_2$ conduction band to the excited dye, leading to a high open-circuit photovoltage (V_{OC}). IAH showed a higher power conversion efficiency (PCE) of 6.90% compared to IDH. Li et al. [24] designed a series of dyes with different π-spacer and acceptor groups. The results showed that the longer conjugated bridge would inhibit the intramolecular charge transfer (ICT). The dye with (E)-3-(4-(benzo[c][1,2,5] thiadiazol-4-yl) phenyl) -2-cyanoacrylic acid (TCA) acceptor group has the higher photoelectrical property due to the lowest chemical hardness, largest electroaccepting power, dipole moment, and the change in the energy of the TiO$_2$ conduction band among the designed dyes. Panneerselvam et al. [43] designed seven TPA molecules with different π-linkers based on two experimentally reported molecules. The results show that furan moieties bring planarity to the molecule and exhibit lower HOMO-LUMO gap. TPA9 exhibits highest absorption maxima. TPA7 has high emission maxima and exhibit planarity in excited state. There is an obvious correlation between optoelectronic properties and HOMO-LUMO gaps. Biswas et al. [44] designed a series of dyes with different π-spacer units. The results show that dye 3 with fused-pyrrole as a spacer will exhibits high efficiency compared to dye 1. The better short-circuit photocurrent (J_{SC}) of dye 3 would be higher than dye 1 due to higher driving force of electrons, singlet excited state lifetime, and the maximum absorption wavelength. Dye 3 will have better open-circuit photovoltage (V_{OC}) than dye 1 due to larger dipole moment.

To reach high efficiency, R. Bobe et al. [45] introduced simple triphenylamine as electron donor, naphthalenediimide (NDI) as the π-spacer embedded between the two thiophene units and cyanoacrylic acid as the electron acceptor to design and synthesize a new sensitizer A1 based on R1, and the molecular structure is shown in Figure 1. The power conversion efficiency (PCE) of A1-sensitized DSSC device reached 6.24, 6.05, and 5.17% using cobalt-, solvent-, and ionic liquid-based redox shuttles, respectively. At the same time, chemical modification on individual units (such as donor, π-spacer and acceptor) is one of the important ways to improve efficiency of DSSCs through the theoretical calculation. Hence, we designed a series of dyes (Figure 1) based on A1 by modifying the donor, π-spacer and acceptor groups. In this work, our aim is to study the influence of tune the A1 structure on the photoelectric parameters, and further, to find good candidates for DSSC applications.
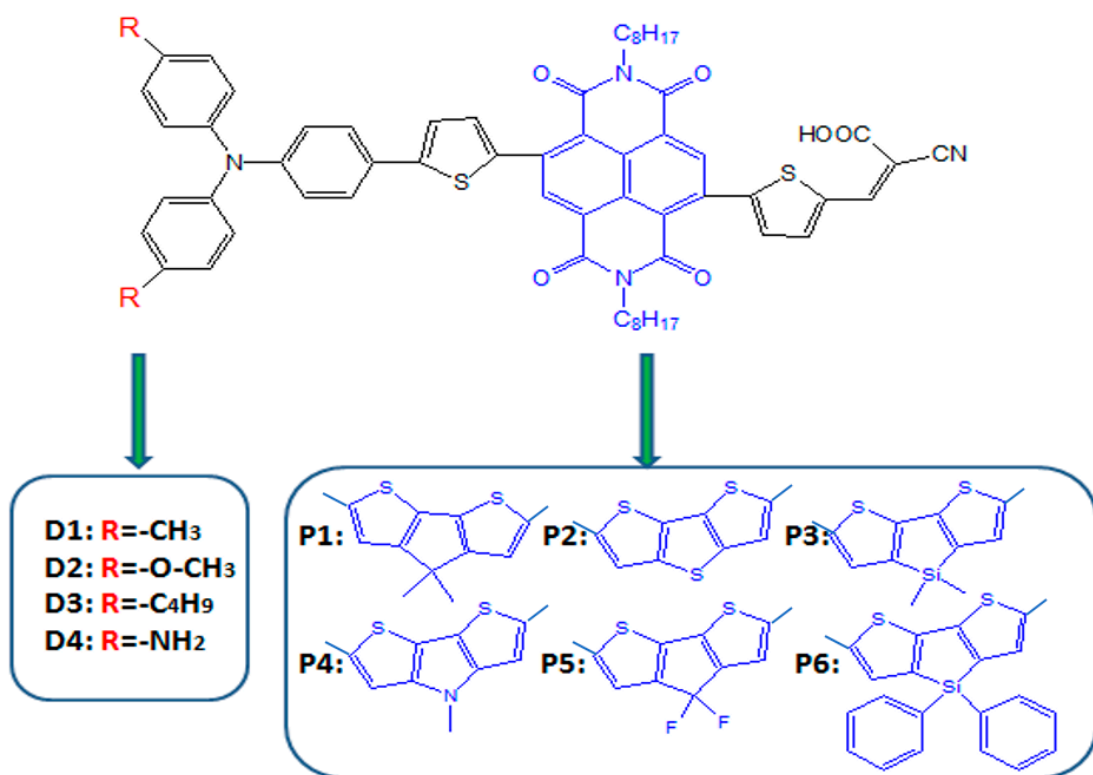
Figure 1. Chemical structure of dyes.

2. Computational Details

2.1. Theoretical Background

As we have known that the sunlight-to-electricity conversion efficiency (η) of DSSCs device is determined by the open-circuit photovoltage (V_{OC}), the short-circuit photocurrent (J_{SC}), the fill factor (FF) and incident solar power on the cell (P_{inc}). η can be described by [46]

$$\eta = FF \frac{V_{OC} J_{SC}}{P_{inc}} \tag{1}$$

In DSSCs, J_{SC} can be determined by the following equation [47]

$$J_{SC} = \int_{\lambda} LHE(\lambda) \phi_{inject} \eta_{collect} d\lambda \tag{2}$$

where $LHE(\lambda)$ is the light harvesting efficiency at a given wavelength, ϕ_{inject} is the electron injection efficiency, and $\eta_{collect}$ denotes the charge collection efficiency. All the components of DSSCs are only different in dyes, hence $\eta_{collect}$ can be assumed to be a constant. $LHE(\lambda)$ can be expressed as

$$LHE = 1 - 10^{-f} \tag{3}$$

where f represents the oscillator strength of dye molecules corresponding to wavelength $\lambda_{\max}$. ϕ_{inject} is related to injection driving force ΔG^{inject} of electrons injecting from the excited dyes to the semiconductor substrate. ΔG^{inject} can be estimated as [48,49]

$$\Delta G^{inject} = E^{dye*} - E_{CB} \tag{4}$$

where E^{dye*} is the oxidation potential of the excited dye and E_{CB} is the conduction band edge of the semiconductor ($E_{CB} = -4.00$ eV). E^{dye*} can be estimated as [50]

$$E^{dye*} = E^{dye} - E_{0-0} \tag{5}$$

where E^{dye} is the redox potential of the ground state of the dye and E_{0-0} is the vertical transition energy associated to the $\lambda_{\max}$. Hence the larger LHE and ΔG^{inject} are benefit to increase J_{SC} value.

In DSSCs, V_{OC} can be expressed by the following equation [50]

$$V_{OC} = \frac{E_{CB} + \Delta E_{CB}}{q} + \frac{k_b T}{q} \ln(\frac{n_c}{N_{CB}}) - \frac{E_{redox}}{q} \tag{6}$$

where q is the unit charge, E_{CB} is the conduction band edge of the semiconductor substrate, $k_b T$ is the thermal energy, n_c is the number of electron in the conduction band, N_{CB} is the density of accessible states in the conduction band and E_{redox} is the electrolyte Fermi level. ΔE_{CB} is the shift of E_{CB} when the dyes are adsorbed on substrate and it can be described by [51]

$$\Delta E_{CB} = -\frac{q\mu_{normal}\gamma}{\varepsilon_0 \varepsilon} \tag{7}$$

In this expression, μ_{normal} is the dipole moment of individual dye perpendicular to the surface of semiconductor substrate, γ denotes the surface concentration of dyes. ε_0 and ε_0 represent the vacuum permittivity and the dielectric permittivity, respectively. It is obvious that μ_{normal} is the key factor determining V_{OC}.

2.2. Computational Detail

The ground state geometries of all the dyes before and after binding to TiO$_2$ in chloroform solvent were fully optimized using density functional theory (DFT) [52] at B3LYP [53] level, 6-31G(d) for nonmetal atoms, while LANL2DZ basis set for Ti atom. The excitation energies, oscillator strengths, and the UV–vis absorption spectra of all the dyes before and after binding to TiO$_2$ in chloroform solvent were simulated using the time-dependent density functional theory (TDDFT) [54] with CAM-B3LYP [55] function, 6-31G(d) basis set for C, H, O, N, S atoms and LANL2DZ basis set for Ti atom on the basis of optimized geometries. However, different exchange–correlation (XC) functionals have a significant effect on the absorption spectra. In order to find a suitable functional, three different XC functionals (CAM-B3LYP, B3PW91, and LC-WPBE) combined with 6-31G(d) basis set are used to calculate absorption spectra in chloroform solvent. The conductor-like polarized continuum model (C-PCM) method is used to simulate the solvent effects. This method was recognized as access reliable results to the experimental values [56]. The calculated results are shown in Figure 2. From the Figure 2, it is obvious that CAM-B3LYP functional is close to the experimental values among five different XC functionals. Kathiravan et al. used CAM-B3LYP to predict the absorption spectra closer to the experimental values compared to other functional [57]. Many previous literatures have shown that CAM-B3LYP can accurately characterize UV–vis absorption spectra [44,58,59]. Therefore, CAM-B3LYP can provide a more reliable and rational description of the UV–vis absorption spectra, and it is used to simulate the absorption properties of dyes before and after binding to TiO$_2$ in chloroform solvent. All calculations were performed with Gaussian 09 package [60].
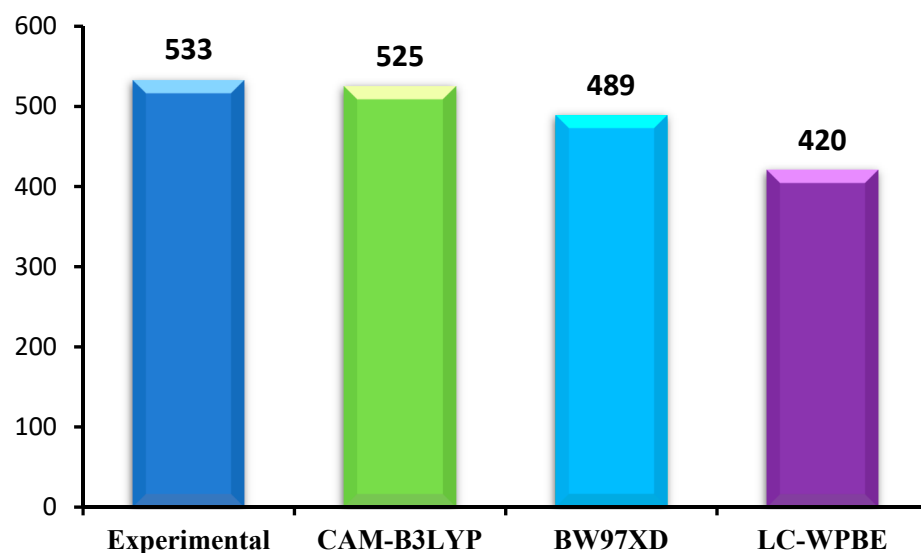
Figure 2. Maximum absorption wavelength (λ_{max}/nm) of A1 in chloroform solution calculated by TD-DFT at different functionals with 6-31G(d) level.

3. Results and Discussion

3.1. Screening of the π-Spacer

The π-linker in D-π-A structured dyes is a key factor to affect charge transfer, light absorption and photophysical properties of dyes. R. Bobe et al. [45] find that the extension of π-linker via the insertion of NDI moiety between the two thiophene units exhibits superior performance. Therefore, we designed a series of D-π-A dyes, which triphenylamine as electron donor, cyanoacrylic acid as electron acceptor, and different thiophene derivatives were inserted between the two thiophene units as π-linker (see Figure 1). Commonly, the conjugation degree is an important parameter that affects the absorption property of the dyes. In order to study the influence of different π-spacers on the degree of conjugation, the ground state structures of dyes were optimized at DFT/B3LYP/6-31G(d) in chloroform solvent, and the selected parameters (bond length and bond angle) are listed in Table 1. The dihedral angles (Φ_1) between the donor and π-spacer are -21.17, 21.30, -20.56, -20.53, -21.06, -18.34, and $22.46°$ for P1–P6 and A1, respectively. This clearly indicates that the dihedral angles (Φ_1) of designed dyes P1–P6 are slightly smaller than that of A1, which means that the conjugation degree of P1–P6 are superior to A1. Hence, introduction of different thiophene derivatives to replace NDI moiety is not only enhance conjugation degree but also inhibit π-aggregation due to the slightly lower the dihedral angle (Φ_1). The favorable conjugation of P1–P6 will increase the delocalization of frontier molecular orbitals (FMOs) and facilitates electron transfer process throughout the molecule. The dihedral angles (Φ_2/Φ_3) between the thiophene derivative and the thiophene are $9.48/0.20$, $-9.82/-1.96$, $7.54/1.84$, $8.76/0.35$, $11.17/4.81$, $8.75/1.33$, and $-37.79°/-118.77°$ for P1–P6 and A1, respectively. It is found that the dihedral angles (Φ_2/Φ_3) of P1–P6 are smaller than that of A1, indicating that after introduction of different thiophene derivatives to replace NDI moiety, the π-spacer more rigid. Generally, dyes with rigid π-spacer exhibit outstanding performance compared with corresponding twistable π-spacer. The dihedral angles (Φ_4) between the π-spacer and acceptor are -179.94, -0.25, -179.72, 179.86, 179.93, -179.92, and $-179.70°$ for P1–P6 and A1, respectively, which are all close to $0°$. This means that donor and acceptor is more in a plan, thereby the excited electrons are more easily transferred from donor to acceptor and finally inject into the TiO_2. Thus, introduction of different thiophene derivatives in π-spacer facilitates electron transition. Table 1 clearly shows that the bond lengths d_1 and d_4 of all dyes have no significant change with different π-spacer. The bond lengths d_2 and d_3 of P1–P6 are in the range of 1.441–1.442 and 1.433–1.438 Å, respectively. There

is no obvious change. Compared to A1, the bond lengths d_2 and d_3 are relatively shortened with introduction of thiophene derivatives in the π-spacer (P1–P6). The shorter bond length is beneficial to facilitate the ICT in the D-π-A molecules [44]. The bond lengths of all dyes are in between C–C single and C=C double bonds.

Table 1. Selected bond lengths (Å) and dihedral angles (°) of triphenylamine derivative dyes in chloroform solvent.

	Φ_1	Φ_2	Φ_3	Φ_4	d_1	d_2	d_3	d_4
A1	22.46	−37.79	−118.77	−179.70	1.460	1.465	1.481	1.425
P1	−21.17	9.48	0.20	−179.94	1.462	1.441	1.433	1.415
P2	21.30	−9.82	−1.96	−0.25	1.461	1.442	1.438	1.419
P3	−20.56	7.54	1.84	−179.72	1.462	1.442	1.435	1.416
P4	−20.53	8.76	0.35	179.86	1.462	1.441	1.433	1.415
P5	−21.06	11.17	4.81	179.93	1.462	1.441	1.436	1.418
P6	−18.34	8.75	1.33	−179.92	1.462	1.442	1.436	1.417
D1	21.74	−38.95	−117.02	−179.63	1.460	1.465	1.482	1.425
D2	23.62	−36.97	−118.20	−179.94	1.459	1.463	1.481	1.425
D3	21.71	−38.04	−115.34	−179.49	1.461	1.464	1.482	1.425
D4	22.15	−36.17	−116.88	−179.67	1.457	1.462	1.481	1.424

Over the years, the energy levels and frontier molecular orbitals (FMOs) are used to obtain information on the electronic excitation and transition properties of dyes [61,62]. The molecular orbital energy diagrams of HOMO−2, HOMO−1, HOMO, LUMO, LUMO+1, and LUMO+2 are computed at DFT/B3LYP/6-31G(d) in chloroform solvent and depicted in Figure 3a. To design effective dyes, the HOMO and LUMO levels of dyes must match to the redox potential of I^-/I_3^- electrolyte and the conduction band (CB) of the TiO$_2$ [36]. The LUMO levels of designed dyes P1–P6 are in the range of −2.98 to −2.79 eV. Those values lie above the conduction band (CB) of the TiO$_2$ (−4.0 eV), indicating that excited state designed dyes P1–P6 could quickly and efficiently electron injections into the TiO$_2$ conduction band. The HOMO levels of designed dyes P1–P6 are in the range of −4.82 to −4.93 eV. Those values are below the redox potential of I^-/I_3^- electrolyte (−4.60 eV) [63], demonstrating that oxidized dyes could quickly get electrons from the electrolyte. According to the above analyses, those dyes are better photosensitizer candidates. As shown in Figure 3a, P1 and P4 (−4.82 eV) have the higher HOMO level, followed by P3 (−4.84 eV), P6 (−4.85 eV), P2 (−4.92 eV), P5 (−4.93 eV), and A1 (−5.08 eV), respectively. It is clearly that the HOMO levels of P1–P6 are up-shifted compared to A1, indicating that introduction of thiophene derivatives to replace NDI moiety has little effect on HOMO level. The HOMO-1 of dyes P1–P6 and A1, lying at about −5.30, −5.44, −5.33, −5.29, −5.43, −5.35, and −6.03 eV (see Table S1), which is about 0.48, 0.52, 0.49, 0.47, 0.50, 0.50, and 0.95 eV below their respective HOMO. The LUMO energy levels are in following the order: P4 (−2.79 eV), P1 (−2.84 eV), P3 (−2.85 eV), P6 (−2.87 eV), P2 (−2.90 eV), P5 (−2.98 eV), and A1 (−3.43 eV), respectively. We can find that the LUMO levels of P1–P6 are up-shifted significantly compared to A1, indicating that introduction of thiophene derivatives to replace NDI moiety has a significant effect on LUMO level. The LUMO+1 of dyes P1–P6 and A1, lying at about −1.85, −1.90, −1.91, −1.76, −2.09, −1.96, and −2.55 eV (see Table S1), which is about 0.99, 1.00, 0.94, 1.03, 0.89, 0.91, and 0.88 eV above that of LUMO. From Figure 3a we can find that the energy gaps between the HOMO and the LUMO of P1–P6 are larger than that of A1 due to the higher LUMO level.
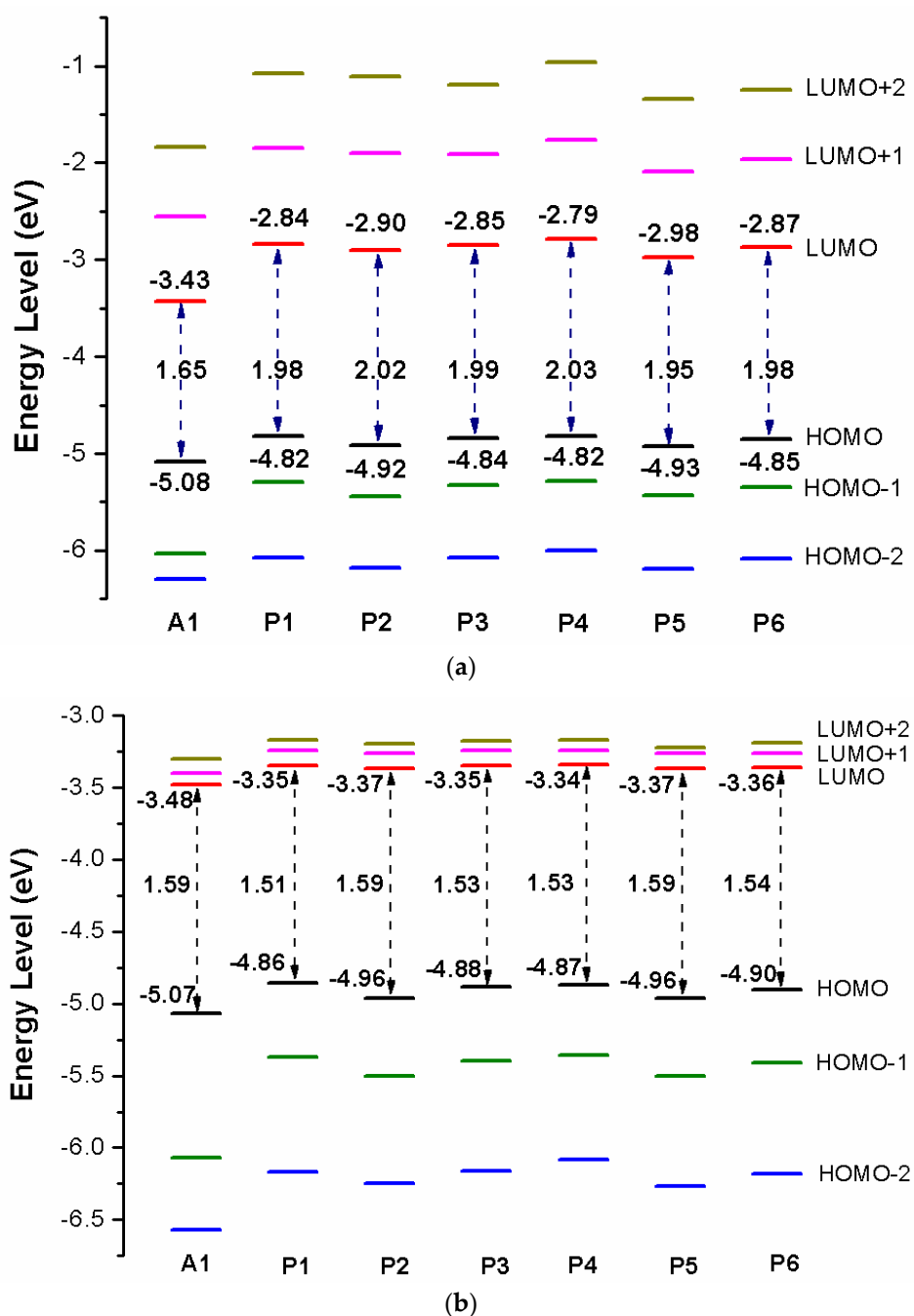
Figure 3. Energy level diagram of (**a**) isolated dyes P1–P6 and A1, (**b**) dyes P1–P6 and A1 after bound to TiO$_2$ surface in chloroform solvent.

In order to clearly see the electron distribution and further understand the relationship between the electronic structure and electron transition. The frontier molecular orbitals diagram (HOMO and LUMO) of P1–P6 and A1 are shown in Figure 4. Figure 4 clearly indicates that the HOMO orbital of A1 is delocalized over donor unit and the left part of π-spacer, while the LUMO orbital of A1 is mainly localized on π-spacer. For dyes P1–P6, the HOMO orbital are concentrated over donor unit and π-spacer, while the LUMO orbital are focused on π-spacer and acceptor unit. To gain more information into the frontier molecular orbitals, the molecular orbital compositions of donor, π-spacer and acceptor for HOMO and LUMO are shown in Figure 5 and the values are listed in Table S2. For dye A1, donor moiety contributes significantly (86%) of HOMO orbital, while π-spacer contributes significantly (92%) of LUMO orbital. For dyes P1–P6, the orbital densities of HOMO

are mainly localized on the donor unit and π-spacer, and the values are 45%(D)/53%(π-spacer), 60%(D)/38%(π-spacer), 51%(D)/47%(π-spacer), 51%(D)/47%(π-spacer), 64%(D)/35%(π-spacer), and 53%(D)/46%(π-spacer), respectively. The orbital densities of LUMO are mainly centered at π-spacer and acceptor unit, and the values are 51%(π-spacer)/49%(A), 54%(π-spacer)/45%(A), 52%(π-spacer)/48%(A), 52%(π-spacer)/48%(A), 58%(π-spacer)/41%(A), and 56%(π-spacer)/43%(A), respectively. This better charge separation of HOMO and LUMO for dyes P1–P6 is benefit to electron injection from the excited dye to the conduction band of the semiconductor. The difference between the molecular orbital compositions (MOC) of acceptor unit was used to study the charge-transfer property. P1 exhibits highest molecular orbital compositions (MOC) difference (47%), followed by P3 = P4 (46%), P2 (43%), P6 (41%), P5 (40%), and A1 (6%), respectively. It is clear that introduction of thiophene derivatives to replace NDI moiety has a significant effect on the difference between the molecular orbital compositions (MOC) of acceptor unit. Therefore, dyes P1–P6 will have more effective intramolecular charge transfer (ICT) upon photoexcitation.
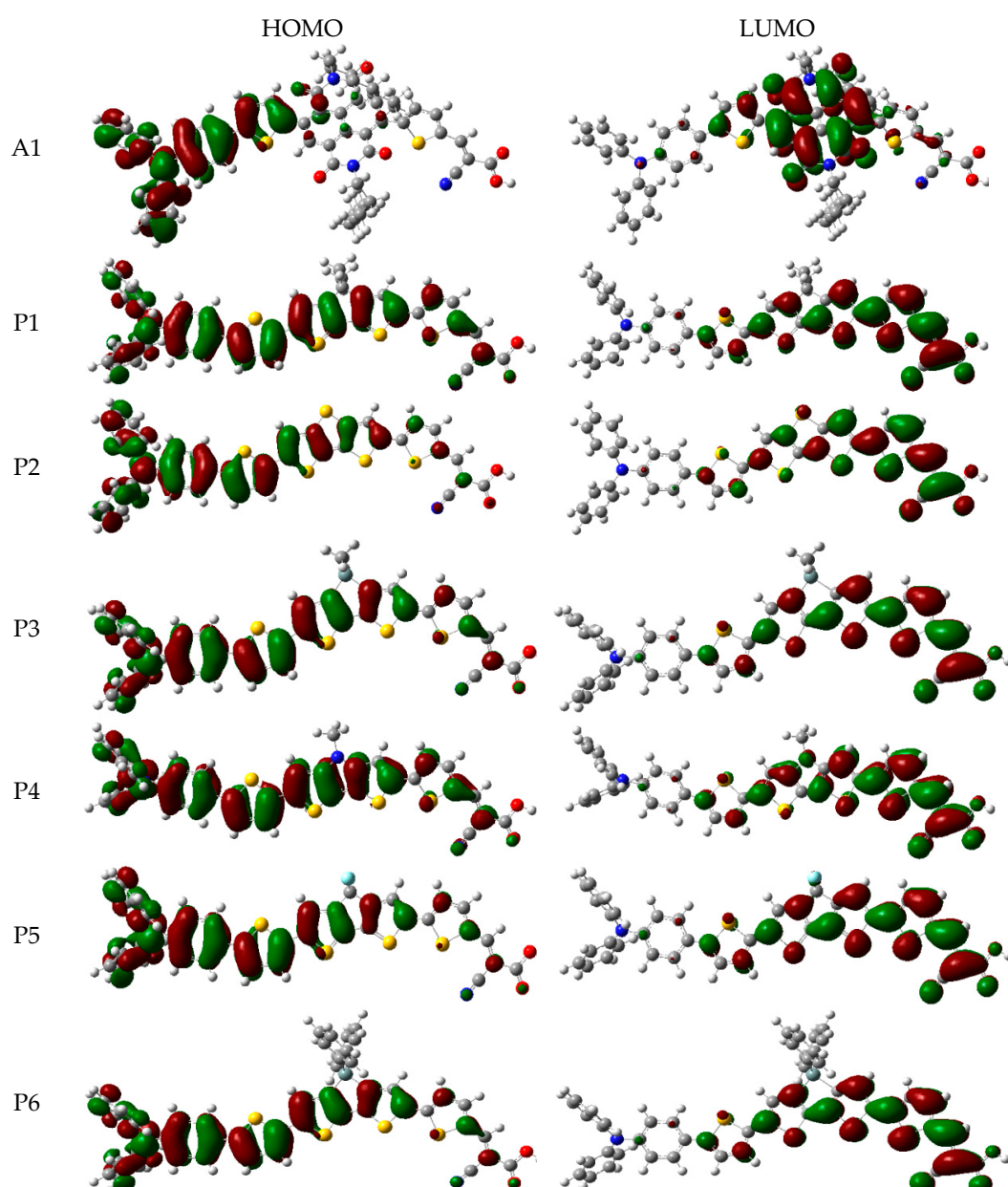

**Figure 4.** Frontier molecular orbitals of dyes P1–P6 and A1 in chloroform solvent.
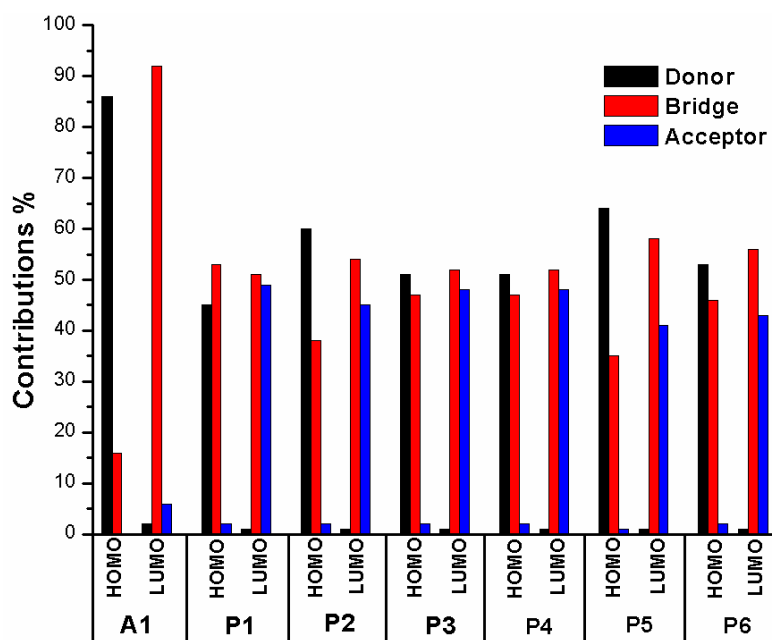
Figure 5. Molecular orbital compositions of the individual groups in HOMO and LUMO of P1–P6 and A1 in chloroform solvent.

After binding on the TiO$_2$ surface, in order to further investigate the electronic coupling between LUMO and the conduction band (CB) of the TiO$_2$, the energy level (HOMO−2, HOMO−1, HOMO, LUMO, LUMO+1, and LUMO+2) of dye was calculated, which were introduced here because some states come from those orbitals and the results are listed in Table S1, the corresponding energy level diagram of the dyes after binding on the TiO$_2$ surface is shown in Figure 3b. The HOMO levels (see Figure 3b) of dyes P1/TiO$_2$–P6/TiO$_2$ and A1/TiO$_2$ are −4.86, −4.96, −4.88, −4.87, −4.96, −4.90, and −5.07 eV, respectively. It is clear that HOMO levels of dyes P1/TiO$_2$–P6/TiO$_2$ have a subtle increase compared to A1/TiO$_2$. The HOMO–1 of dyes P1/TiO$_2$–P6/TiO$_2$ and A1/TiO$_2$, lying at about, −5.37, −5.50, −5.40, −5.36, −5.50, −5.41, and −6.07 eV (see Table S1), which is about 0.51, 0.54, 0.52, 0.49, 0.54, 0.51, and 1.00 eV below their respective HOMO. Compared to the isolated dyes, the HOMO and HOMO-1 levels of dyes/TiO$_2$ are almost unchanged. The LUMO levels (see Figure 3b) of dyes P1/TiO$_2$–P6/TiO$_2$ and A1/TiO$_2$ are −3.35, −3.37, −3.35, −3.34, −3.37, −3.36, and −3.48 eV, respectively, indicating that the LUMO levels have no obvious change. The LUMO+1 levels of dyes P1/TiO$_2$–P6/TiO$_2$ and A1/TiO$_2$, lying at about −3.24, −3.26, −3.24, −3.24, −3.26, −3.26, and −3.40 eV (see Table S1), there is no obvious change compared to their LUMO levels. Compared to the isolated dyes, the LUMO level of A1/TiO$_2$ has no obvious change. For P1/TiO$_2$–P6/TiO$_2$, the LUMO levels are down-shifted significantly compared to isolated dyes P1–P6. The LUMO+1 levels of dyes P1/TiO$_2$–P6/TiO$_2$ and A1/TiO$_2$ are also down-shifted significantly compared to isolated dyes. The energy gaps of dyes P1/TiO$_2$–P6/TiO$_2$ and A1/TiO$_2$ are in the range of 1.51 to 1.59 eV, there is no obvious change (Figure 3b). After binding on the TiO$_2$ surface, HOMO levels of P1/TiO$_2$–P6/TiO$_2$ have no obvious change compared to the isolated dyes, while the LUMO levels of P1/TiO$_2$–P6/TiO$_2$ are down-shifted significantly compared to isolated dyes, which leads to energy gaps decrease by 0.47, 0.43, 0.46, 0.50, 0.36, and 0.44 eV for P1/TiO$_2$–P6/TiO$_2$ compared to their isolated dyes (see Figure 3b), and the energy gap of A1/TiO$_2$ has minor change compared to its isolated dyes. Once the dyes binding on the TiO$_2$ surface, the energy levels of dyes will change due to bonding mechanism between the semiconductor conduction band and dye, therefore, some photoelectric properties of dyes/TiO$_2$ will change compared to dye.

In order to predict and explain chemical reactions (such as hydrogen bonding interactions), molecular electrostatic potential (MEP) were calculated at B3LYP/6-31G(d), which has a close

relationship with the electron cloud, and the result are shown in Figure 6. Molecular electrostatic potential (MEP) is used to describe the nucleophilic and electrophilic reaction sites. The different colors at the surface represent different electrostatic potential values. The red (negative) color area of the molecular electrostatic potential (MEP) depicts electrophilic reactivity, which refer to electron-rich areas. While blue (positive) color area depicts nucleophilic reactivity, which refer to electron-poor areas. The values of electrostatic potential are in increasing order: red < orange < yellow < green < blue. The color code of molecular electrostatic potential (MEP) maps ranges from -0.06 a.u. (deepest red) to 0.06 a.u. (deepest blue). Figure 6 indicates that the most positive potential is observed on carboxyl hydrogen atom, which is preferred area for nucleophilic attack. The greatest negative potential is found on nitrogen atom of -CN group, which is the preferred site of electrophilic attack.


A1   P1

P2   P3

P4   P5

P6
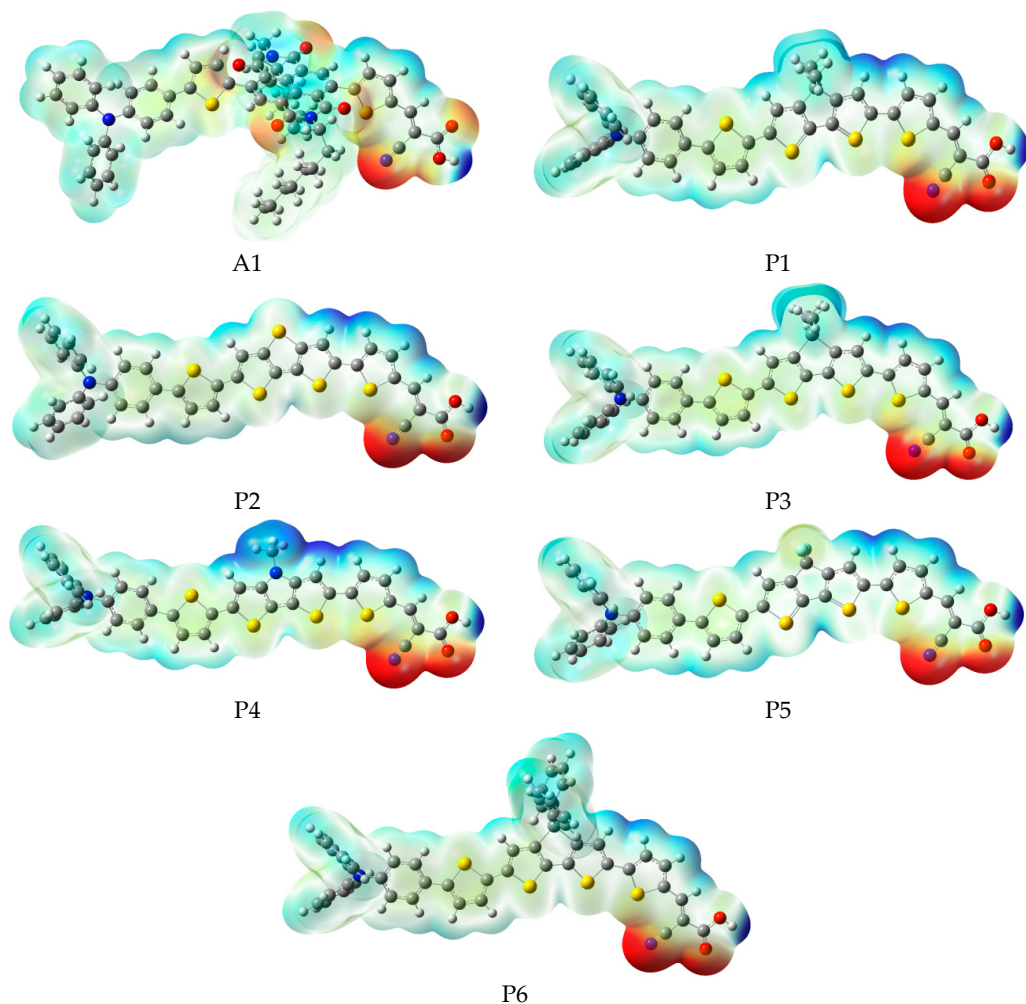
Figure 6. Molecular electrostatic potential plots of dyes P1–P6 and A1 in chloroform solvent.

Over the years, time-dependent DFT (TD-DFT) has been widely used in simulation of absorption and emission spectra [64]. Therefore, absorption spectra of dyes P1–P6 and A1 were calculated by using TD-DFT//Cam-B3LYP/6-31G(d) method based on the geometry optimization of the ground state. The functional selection is discussed in Section 2.2. The calculated oscillator strengths (f), excitation energies (E_g), maximum absorption wavelengths (λ_{max}), and main electron transition are listed in Table 2, and the UV–vis absorption spectra with DFT results are shown in Figure 7. Table 2 illustrates that the first excited states of dyes P1–P6 and A1 show the same electronic transition from HOMO to LUMO. The maximum absorption peaks (λ_{max}) of the dyes P1–P6 and A1 are found at 505–549 nm, which are all in visible region (see Figure 7a). It is the important region for photo-to-current conversion.

The maximum absorption peaks ($\lambda_{\max}$) of dyes are in following order; P1 (549 nm) > P3 (541 nm) = P5 (541 nm) > P6 (540 nm) > P4 (535 nm) > A1 (525 nm) > P2 (505 nm). Compared to A1, it is clear that only P2 shows blue shift by 20 nm. P1, P3, P4, P5, and P6 show red shift by 24, 16, 16, 15, and 10 nm, respectively. The red-shift of the absorption peak is beneficial to improve the open-circuit photovoltage (V_{OC}) and short-circuit photocurrent (J_{SC}), which leads to a higher photoelectric conversion efficiency (PCE) of the DSSC. Absorption spectra (see Figure 7a) shows that P1–P6 exhibit a broad absorption band compared to A1 in the visible region, which is beneficial for improving the efficiency. After binding on the TiO$_2$ surface, absorption properties (such as maximum absorption peak and oscillator strength) of the dyes/TiO$_2$ were obviously changed due to the interaction between the dyes and the TiO$_2$. The electronic and optical parameters of dyes/TiO$_2$ are listed in Table 2, and the absorption spectra are shown in Figure 7b. The maximum absorption peaks ($\lambda_{\max}$) of dyes/TiO$_2$ are in following order; P1/TiO$_2$ (601 nm) > P3/TiO$_2$ (586 nm) > P4/TiO$_2$ (585 nm) > P5/TiO$_2$ (581 nm) > P6/TiO$_2$ (572 nm) > P2/TiO$_2$ (543 nm) > A1/TiO$_2$ (529 nm). It is clear that dyes P1–P6 show a significant red-shift compared to A1, and the values are 72, 57, 56, 52, 43, and 14 nm, respectively. The first excited states of all the dye/TiO$_2$ show a major contribution from HOMO to LUMO. Compared to the isolated dyes, the maximum absorption peak ($\lambda_{\max}$) is 52, 38, 45, 50, 40, 32, and 4 nm red-shift for dyes P1/TiO$_2$–P6/TiO$_2$ and A1/TiO$_2$, respectively. To analyze the charge transfer properties of the excited state for dyes/TiO$_2$, the charge difference density (CDD) are shown in Figure 8, where the green and red color stand for an increase and a decrease of electronic density, respectively. As depicted in Figure 8, for A1/TiO$_2$, the density increment region of the excited state S1, S2, and S3 is mostly located on NDI moiety, while the density depletion zone is mainly distributed on donor group. For P1/TiO$_2$-P6/TiO$_2$, the electronic density of the excited state S1 shows a decrease at π-spacer and a increase at the π-spacer and acceptor moiety, the electronic density of the excited state S2 shows a decrease at donor and π-spacer and a increase at the π-spacer, acceptor and TiO$_2$. For the excited state S3, evidently, the electronic density of P1/TiO$_2$ and P4/TiO$_2$ are all located on TiO$_2$, while the density increment zone for P2/TiO$_2$, P3/TiO$_2$, and P6/TiO$_2$ is mostly located on TiO$_2$ and rest electronic density is located on acceptor moiety. The electronic density of P5/TiO$_2$ is all located on the π-spacer and acceptor moiety. In summary, the electrons in the excited state S6 for P1/TiO$_2$–P4/TiO$_2$ and P6/TiO$_2$ are in direction form dye to TiO$_2$.

Table 2. Computed excitation energy (E_g/eV), maximum absorption wavelength ($\lambda_{\max}$/nm), oscillator strength (f), and electronic transition configuration of triphenylamine derivative dyes in chloroform solution.

Dye	State	E_g/$\lambda_{\max}$	f	Main Configurations
A1	1	2.36/525	0.7597	H → L/0.58940
	2	3.26/380	0.1511	H-2 → L/0.43402
	3	3.43/362	0.2330	H-2 → L/0.40002
P1	1	2.26/549	2.2053	H → L/0.59065
	2	3.15/393	0.3574	H → L + 1/0.51442
	3	3.58/347	0.0434	H-1 → L/0.37490
P2	1	2.45/505	2.2594	H → L/0.51866
	2	3.21/386	0.4115	H → L + 1/0.48619
	3	3.66/338	0.1640	H → L/0.42560
P3	1	2.29/541	1.9759	H → L/0.56296
	2	3.15/394	0.4839	H → L + 1/0.49594
	3	3.56/348	0.0119	H → L/0.36012
P4	1	2.32/535	2.3560	H → L/0.59699
	2	3.20/388	0.4152	H → L + 1/0.53467
	3	3.59/345	0.0676	H-2 → L/0.57213
P5	1	2.29/541	2.0460	H → L/0.52808
	2	3.14/395	0.1942	H → L + 1/0.45139
	3	3.50/354	0.0343	H-1 → L + 1/0.37664

Table 2. *Cont.*

| Dye	State	$E_g/\lambda_{\max}$	f	Main Configurations	
P6	1	2.29/540	1.9468	H →	L/0.55318
	2	3.13/396	0.5035	H →	L + 1/0.48466
	3	3.54/351	0.0117	H →	L/0.36083
D1	1	2.32/534	0.7459	H →	L/0.59261
	2	3.24/382	0.1267	H-1 →	L/0.46484
	3	3.40/365	0.1976	H-2 →	L/0.48305
D2	1	2.26/548	0.7609	H →	L/0.59379
	2	3.18/390	0.1150	H-1 →	L/0.48838
	3	3.37/368	0.2005	H-2 →	L/0.52160
D3	1	2.33/532	0.7493	H →	L/0.58869
	2	3.24/382	0.1095	H-1 →	L/0.47235
	3	3.39/365	0.1981	H-2 →	L/0.50056
D4	1	2.17/571	0.7540	H →	L/0.59999
	2	3.06/405	0.1200	H-1 →	L/0.51377
	3	3.36/369	0.1856	H-3 →	L/0.55893
A1/TiO$_2$	1	2.34/529	0.7923	H →	L/0.58409
	2	3.23/384	0.5380	H-1 →	L/0.36516
	3	3.38/366	0.4640	H →	L/0.37280
P1/TiO$_2$	1	2.06/601	2.6104	H →	L/0.54964
	2	3.02/411	0.2565	H →	L + 16/0.35495
	3	3.29/376	0.0087	H →	L + 1/00.55205
P2/TiO$_2$	1	2.28/543	2.5567	H →	L/0.48438
	2	3.12/398	0.3216	H →	L + 16/0.36183
	3	3.46/359	0.2092	H →	L/0.43632
P3/TiO$_2$	1	2.12/586	2.3440	H →	L/0.51644
	2	3.02/410	0.4186	H-1 →	L/0.32626
	3	3.33/372	0.0355	H →	L/0.41457
P4/TiO$_2$	1	2.12/585	2.7395	H →	L/0.53415
	2	3.09/401	0.2884	H-1 →	L/0.32472
	3	3.30/376	0.0030	H →	L + 1/0.57187
P5/TiO$_2$	1	2.13/581	2.4142	H →	L/0.50933
	2	3.01/412	0.1571	H-1 →	L/0.34133
	3	3.32/373	0.0276	H →	L/0.41752
P6/TiO$_2$	1	2.17/572	2.2638	H →	L/0.49491
	2	3.04/407	0.4603	H-2 →	L/0.30426
	3	3.36/369	0.0316	H →	L/0.45448
D1/TiO$_2$	1	2.31/538	0.7861	H →	L/0.59277
	2	3.26/380	0.2399	H-1 →	L/0.48023
	3	3.38/367	0.8011	H-2 →	L + 4/0.35860
D2/TiO$_2$	1	2.24/553	0.7936	H →	L/0.59502
	2	3.19/388	0.1238	H-1 →	L/0.51121
	3	3.38/367	0.9464	H-3 →	L/0.41438
D3/TiO$_2$	1	2.31/538	0.7819	H →	L/0.58538
	2	3.21/387	0.3757	H-1 →	L/0.44284
	3	3.35/370	0.6066	H-2 →	L + 4/0.30048
D4/TiO$_2$	1	2.13/581	0.8108	H →	L/0.59550
	2	3.01/411	0.2016	H-1 →	L/0.50064
	3	3.26/380	0.4754	H →	L + 4/0.37904

(a)

(b)
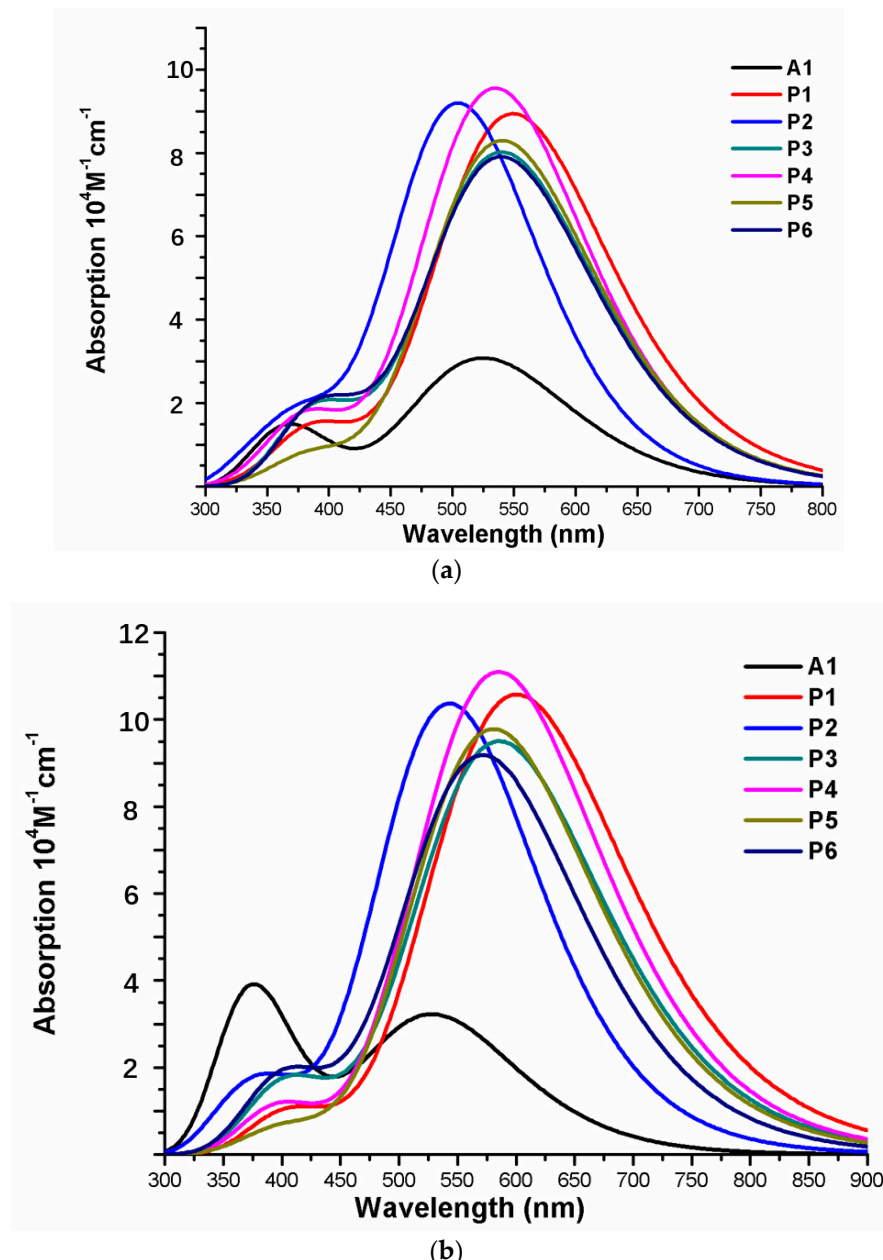
Figure 7. Absorption spectra of (**a**) isolated dyes P1–P6 and A1, (**b**) dyes P1–P6 and A1 after bound to TiO$_2$ surface in chloroform solvent.

The emission properties (fluorescence energies, the emission peaks and oscillator strengths and) of the dyes P1–P6 and A1 were calculated at the TD-DFT//CAM-B3LYP/6-31G(d) level in chloroform solution, and the results are listed in Table 3. As shown in Table 3, the maximum emission wavelengths (λ_{em}) of dyes exhibit higher wavelengths (~100 nm) than their maximum absorption wavelengths (λ_{max}). P5 has largest λ_{em} at 685 nm which is 144 nm higher than its λ_{max}, while P2 has lowest λ_{em} with 610 nm, which is 105 nm higher than its λ_{max}. The maximum emission wavelengths (λ_{em}) of dyes are in following order; P5 > A1 > P6 > P3 > P1 > P4 > P2. All dyes exhibit same electronic transition from HOMO to LUMO. Compared to A1, the maximum emission wavelength of P6 shows red shift by 9 nm while P1–P5 show blue shift by 6, 66, 11, 56, and 8 nm, respectively. P6 can be used as efficient blue-light-emitting materials due to larger oscillator strength and the emission peak.
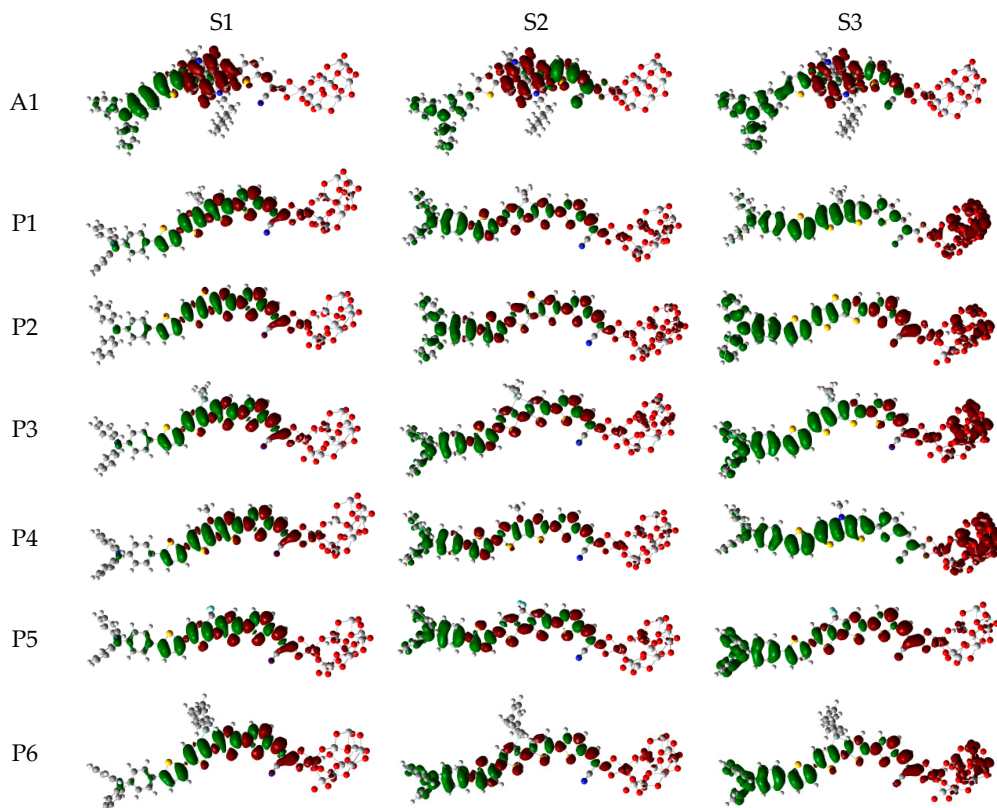
Figure 8. Charge difference density (CDD) of the selected excited state for dyes P1–P6 and A1 after bound to TiO$_2$ surface in chloroform solvent.

Table 3. Emission properties of triphenylamine derivative dyes in chloroform solvent.

Dye	State	E_{flu}(eV)/λ_{em}(nm)	f	Main Configurations	
A1	1	1.84/676	0.7606	H $\rightarrow$	L/0.64473
P1	1	1.87/662	2.3909	H $\rightarrow$	L/0.65705
P2	1	2.03/610	2.4533	H $\rightarrow$	L/0.62022
P3	1	1.86/665	2.1311	H $\rightarrow$	L/0.64954
P4	1	2.00/620	2.5404	H $\rightarrow$	L/0.64919
P5	1	1.81/685	2.1693	H $\rightarrow$	L/0.64219
P6	1	1.86/668	2.0739	H $\rightarrow$	L/0.64715
D1	1	1.81/685	0.7513	H $\rightarrow$	L/0.64168
D2	1	1.78/697	0.7130	H $\rightarrow$	L/0.63564
D3	1	1.81/685	0.7540	H $\rightarrow$	L/0.64135
D4	1	1.72/723	0.7148	H $\rightarrow$	L/0.62513

To better predict the short-circuit photocurrent (J_{SC}) of dyes, light harvesting efficiency (LHE) and the driving force of electron injection (ΔG^{inject}) are calculated, and the results are listed in Table 4. According to Equation (3), it is clear that light harvesting efficiency (LHE) is related to the oscillator strength (f). In order to obtain larger light harvesting efficiency (LHE), the oscillator strength (f) should be as higher as possible. The oscillator strengths (f) of dyes P1–P6 are 2.2053, 2.2594, 1.9759, 2.3560, 2.0460, and 1.9468 (see Table 2), respectively, which are much higher than that of A1 (0.7597). Therefore, light harvesting efficiency (LHE) of dyes P1–P6 are larger than that of A1, and the values are in following order; P4 (0.996) > P1 (0.994) = P2 (0.994) > P5 (0.991) > P3 (0.989) = P6 (0.989) > A1 (0.826). The results show that introduction of thiophene derivatives to replace NDI moiety promote light harvesting efficiency (LHE) increase. Hence dyes P1–P6 can absorb more photons, which is beneficial for improving short-circuit photocurrent (J_{SC}). Another factor that influences short-circuit photocurrent (J_{SC}) is driving force of electron injection (ΔG^{inject}). As shown in Table 4, the values of

ΔG^{inject} were negative, indicating that excited state dye lies above the conduction band (CB) of the TiO$_2$, and thus promote electron injection from the excited sensitizer to the TiO$_2$ conduction band. The calculated driving force of electron injection (ΔG^{inject}) are in following order; A1 > P5 > P1 = P6 > P3 > P4 > P2. Dyes P1–P6 exhibit more negative driving force of electron injection (ΔG^{inject}) than that of A1, suggesting that dyes P1–P6 will exhibit faster electron injection. At the same time, the ϕ_{inj} of dyes P1–P6 are larger than that of MA-2 due to their more negative driving force of electron injection (ΔG^{inject}). Therefore, dyes P1–P6 will exhibit larger short-circuit photocurrent (J_{SC}) than that of A1 according to Equation (2). The reorganization energy (ΔG_{reg}) is another important factor that affects the short-circuit photocurrent (J_{SC}) of the DSSCs. Lower reorganization energy (ΔG_{reg}) will lead to faster electron transfer. The reorganization energy (ΔG_{reg}) can be expressed as [65];

$$\Delta G_{reg} = E(I_3^- / I^-) - E_{dye} \tag{8}$$

where $E(I_3^- / I^-)$ is the redox potential (-4.60 eV). As shown in Table 4, the reorganization energy (ΔG_{reg}) of dyes P1–P6 are in the range of 0.22 to 0.33 eV, which are lower than A1 (0.48 eV). Hence dyes P1–P6 will have higher power conversion efficiency due to the lower reorganization energy (ΔG_{reg}) [66]. Above all, introduction of thiophene derivatives to replace NDI moiety can improve short-circuit photocurrent (J_{SC}).

Table 4. Calculated electronic properties of triphenylamine derivative dyes.

Dye	LHE	ΔG^{inject}	E_{dye*}	E_{dye}	ΔG_{reg}	eV_{OC}
A1	0.826	−1.28	2.72	5.08	0.48	0.57
P1	0.994	−1.44	2.56	4.82	0.22	1.16
P2	0.994	−1.53	2.47	4.92	0.32	1.10
P3	0.989	−1.45	2.55	4.84	0.24	1.15
P4	0.996	−1.50	2.50	4.82	0.22	1.21
P5	0.991	−1.36	2.64	4.93	0.33	1.02
P6	0.989	−1.44	−2.56	4.85	0.25	1.13
D1	0.820	−1.34	2.66	4.98	0.38	0.58
D2	0.827	1.39	2.61	4.87	0.27	0.60
D3	0.822	−1.35	2.65	4.98	0.38	0.58
D4	0.824	−1.49	2.51	4.68	0.08	0.63
A1/TiO$_2$	0.839	−1.23	−2.77	5.07	0.47	0.52
P1/TiO$_2$	0.998	−1.20	−2.80	4.86	0.22	0.65
P2/TiO$_2$	0.997	−1.32	−2.68	4.96	0.36	0.63
P3/TiO$_2$	0.995	−1.24	−2.76	4.88	0.28	0.65
P4/TiO$_2$	0.998	−1.25	−2.75	4.87	0.27	0.66
P5/TiO$_2$	0.996	−1.17	−2.83	4.96	0.36	0.63
P6/TiO$_2$	0.995	−1.27	−2.73	4.90	0.30	0.64
D1/TiO$_2$	0.836	−2.39	1.61	4.99	0.39	0.56
D2/TiO$_2$	0.839	−2.51	1.49	4.87	0.27	0.57
D3/TiO$_2$	0.835	−1.33	2.67	4.98	0.38	0.53
D4/TiO$_2$	0.845	−1.45	2.55	4.68	0.08	0.57

In order to analyze the relationship between the LUMO and open-circuit photovoltage (V_{OC}), V_{OC} can be approximately expressed by the formula [67]

$$eV_{OC} = E_{LUMO} - E_{CB} \tag{9}$$

In order to obtain larger eV_{OC}, E_{LUMO} should be as higher as possible [68,69]. As shown in Table 4, the eV_{OC} values of dyes are in following order; P4 (1.21eV) > P1 (1.16 eV) > P3 (1.15 eV) > P6 (1.13 eV) > P2 (1.10 eV) > P5 (1.02 eV) > A1 (0.57 eV). It is clear that dyes P1–P6 should have a larger V_{OC} compared to A1. Introduction of thiophene derivatives to replace NDI moiety not only increases short-circuit photocurrent (J_{SC}), but also enhances open-circuit photovoltage (V_{OC}).

After binding on the TiO$_2$ surface, the oscillator strengths (f) of dyes P1/TiO$_2$-P6/TiO$_2$ are in the range of 2.7395 to 2.2638, which are greatly higher than that of A1/TiO$_2$ (0.7923) (see Table 2).

The light harvesting efficiency (LHE) can be calculated according to Equation (3), and the light harvesting efficiency (LHE) values of dyes/TiO$_2$ are in following order; P1/TiO$_2$ = P4/TiO$_2$ > P2/TiO$_2$ > P5/TiO$_2$ > P3/TiO$_2$ = P6/TiO$_2$ > A1/TiO$_2$. Hence dyes P1/TiO$_2$–P6/TiO$_2$ can absorb more photons compared to A1/TiO$_2$. The oscillator strengths (f) of dyes/TiO$_2$ are larger than that of the isolated dyes (see Table 2), which leads to higher light harvesting efficiency (LHE) compared to the isolated dyes (see Table 3). The driving force of electron injection (ΔG^{inject}) of dyes P1/TiO$_2$-P6/TiO$_2$ are in the range of −1.17 to −1.32 eV, there is no obvious change compared to A1/TiO$_2$ (−1.23 eV). Compared to the isolated dyes, the driving force of electron injection (ΔG^{inject}) of dyes/TiO$_2$ decreases slightly. The reorganization energy (ΔG_{reg}) of dyes/TiO$_2$ are in following order; A1/TiO$_2$ > P2/TiO$_2$ = P5/TiO$_2$ > P6/TiO$_2$ >P3/TiO$_2$ >P4/TiO$_2$ > P1/TiO$_2$. Therefore, dyes P1/TiO$_2$-P6/TiO$_2$ will have higher power conversion efficiency due to the lower reorganization energy (ΔG_{reg}). Compared to the isolated dyes, the reorganization energy (ΔG_{reg}) of dyes/TiO$_2$ has no obvious change. The eV_{OC} values of dyes are in the range of 0.63 to 0.66 eV, which are slightly higher than that of A1/TiO$_2$ (0.52 eV). The eV_{OC} value of A1 has no obvious change before and after binding on the TiO$_2$ surface. For dyes P1–P6, the eV_{OC} values of dyes/TiO$_2$ are slightly lower than that of isolated dyes.

3.2. Screening of the Donors

On the basis of A1, we designed four dyes (see Figure 1) by introducing different electron-donating groups on the triphenylamine donor of A1 (such as $-CH_3$, $-NH_2$, $-OCH_3$, and $-C_4H_9$). As shown in Table 1, it is clear that the dihedral angles (Φ_1, Φ_2, Φ_3, and Φ_4) and bond lengths (d_1, d_2, d_3, and d_4) of dyes D1–D4 have no obvious change compared to A1, which means that introduction different electron-donating groups on the triphenylamine donor of A1 has no obvious effect on dihedral angles and bond lengths.

Figure 9a shows the energy level diagrams of dyes D1–D4 and A1 in chloroform solvent. The LUMO levels of designed dyes D1–D4 are −3.42, −3.40, −3.42, and −3.37 eV, respectively, which are higher than conduction band (CB) of the TiO$_2$ (−4.0 eV). Therefore, electron injection can easily take place from the excited dyes to the TiO$_2$ conduction band. Compared to A1 (−3.43 eV), the LUMO levels of dyes D1–D4 are in the range of −3.42 to −3.37 eV, which have no obvious change. Introduction different electron-donating groups on the triphenylamine donor of A1 have no obvious effect on LUMO level. The LUMO+1 of dyes D1–D4, lying at about −2.65, −2.64, −2.65, and −2.63 eV, (see Table S3), which is about 0.77, 0.76, 0.77, and 0.74 eV above that of LUMO. The HOMO levels of designed dyes D1–D4 are −4.98, −4.87, −4.98, and −4.68 eV, respectively, which are lower than redox potential of I^-/I_3^- electrolyte (−4.60 eV). Hence oxidized dyes could quickly get electrons from the electrolyte. Compared to A1 (−5.08 eV), the HOMO levels of dyes D1–D4 are in the range of −4.98 to −4.68 eV, which have a suitable up-shift. In particular, introduction $-OCH_3$ (D2) and $-NH_2$ (D4) groups on the triphenylamine donor of A1 have a significant on HOMO level. The HOMO-1 of dyes D1–D4, lying at about −6.00, −5.88, −5.99, and −5.71 eV, (see Table S1), which is about 1.02, 1.01, 1.01, and 1.03 eV below their respective HOMO. The energy levels (HOMO and LUMO) of dyes D1–D4 match the redox potential of the I^-/I_3^- couple and the conduction band edge level of TiO$_2$. Hence dyes D1–D4 are suitable candidates for DSSCs. The energy gap between highest occupied molecular orbitals (HOMOs) and lowest unoccupied molecular orbitals (LUMOs) is an important factor affecting power conversion efficiency when the free energy of the transition, which directs the rate of charge transfer (CT). A smaller energy gap can generate more electrons in the visible and exhibits high extinction, leading to higher open-circuit photovoltage (V_{OC}) for better PCE of DSSCs. From Figure 9a the energy gaps between the HOMO and the LUMO of D1–D4 are lower than that of A1 due to the decrease of HOMO energy levels.

The frontier molecular orbitals diagram (HOMO and LUMO) of D1–D4 and A1 are shown in Figure 10. It is obvious that the HOMO orbital of D1–D4 is delocalized over donor unit and the left part of π-spacer, while the LUMO orbital of D1–D4 is mainly localized on π-spacer. D1–D4 have similar electron densities, indicating that introduction of different electron-donating

groups has no significant effect on frontier molecular orbital. To gain more information into the frontier molecular orbitals, the molecular orbital compositions of donor, π-spacer, and acceptor for HOMO and LUMO are shown in Figure 11 and the values are listed in Table S2. For HOMO, the orbital densities of D1–D4 are mainly localized on the D part, while a very small amount of orbital densities are focused in π-spacer part, and the values are 90%(D)/10%(π-spacer), 90%(D)/10%(π-spacer), 99%(D)/1%(π-spacer), and 94%(D)/5%(π-spacer), respectively. Compared to A1 86%(D)/16%(π-spacer), it is clear that orbital densities of D part increase, while orbital densities of π-spacer part decrease after introduction different electron-donating groups on the triphenylamine donor. For LUMO, the orbital densities of D1–D4 are mainly localized on the π-spacer part, while a small amount of orbital densities are focused in A part, and the values are 86%(D)/13%(π-spacer), 86%(D)/12%(π-spacer), 86%(D)/13%(π-spacer), and 84%(D)/13%(π-spacer), respectively. Compared to A1 92%(D)/6%(π-spacer), it is clear that orbital densities of π-spacer part decrease, while orbital densities of A part increase after introduction different electron-donating groups on the triphenylamine donor. D1, D3, and D4 have highest MOC difference (13%), followed by D2 (12%), which are higher than that of A1 (6%). Hence, D1–D4 exhibit better charge-transfer property compared to A1.
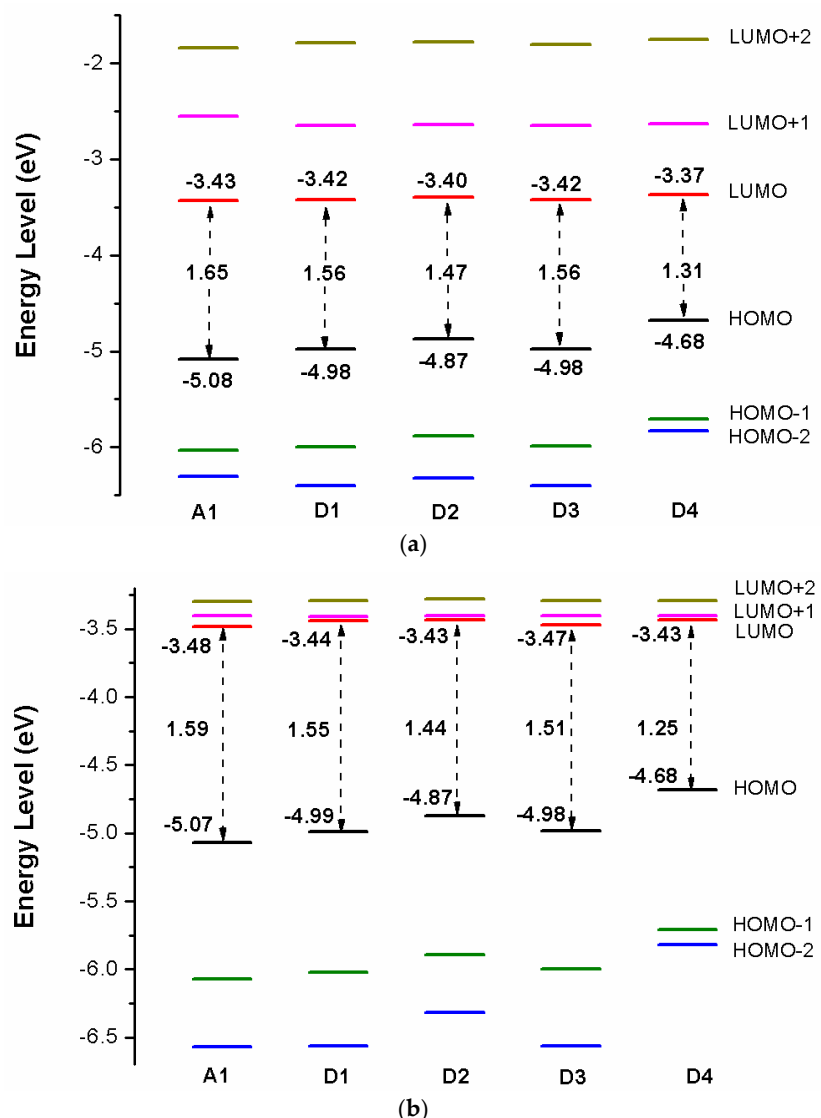
Figure 9. Energy level diagram of (**a**) isolated dyes D1–D4 and A1, (**b**) dyes D1–D4 and A1 after bound to TiO$_2$ surface in chloroform solvent.
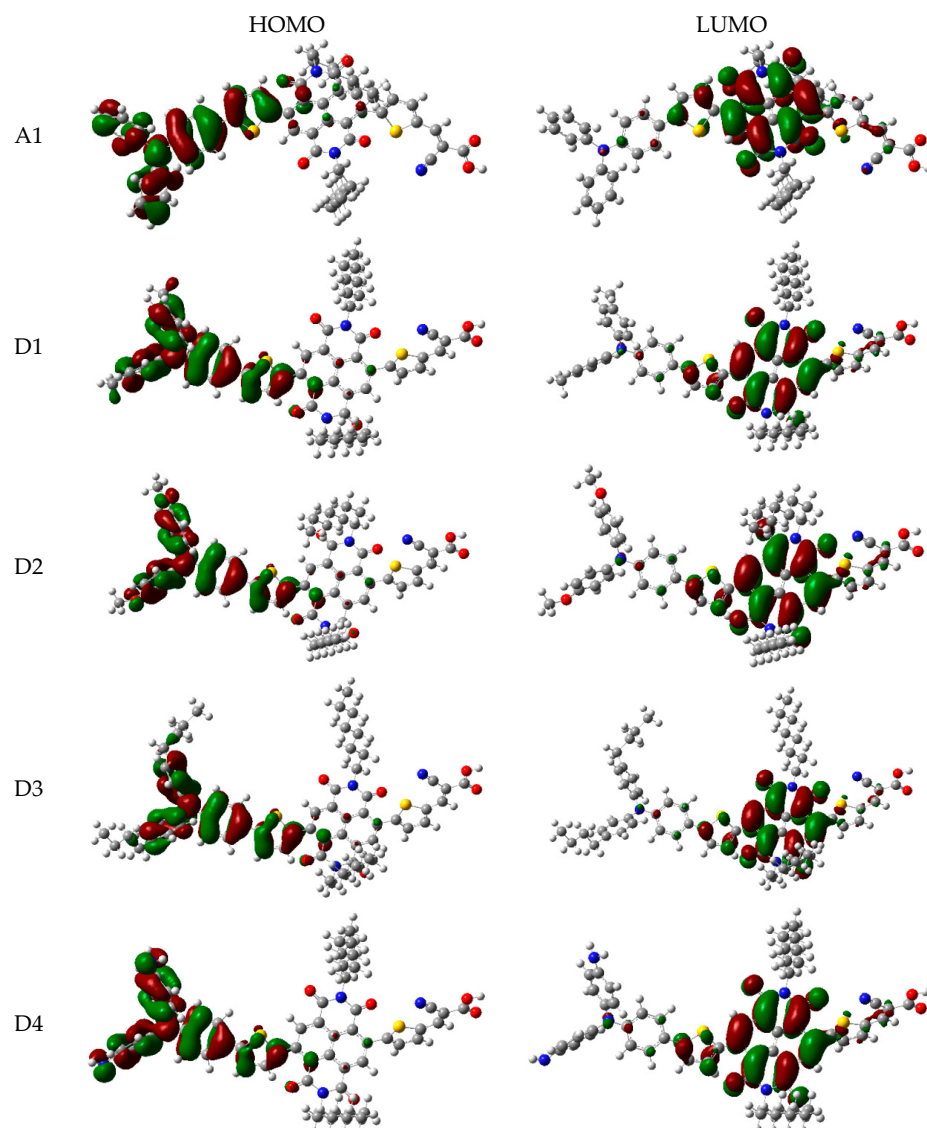
Figure 10. Frontier molecular orbitals of dyes D1–D4 and A1 in chloroform solvent.

After binding on the TiO$_2$ surface, the energy level of dye was calculated, and the results are listed in Table S1, the corresponding energy level diagram is shown in Figure 9b. The HOMO levels (see Figure 9b) of dyes D1/TiO$_2$–D4/TiO$_2$ are −4.99, −4.87, −4.98, and −4.68 eV, respectively. Compared to A1/TiO$_2$ (−5.07 eV), D1 and D3 have no obvious change, D2 and D4 have a subtle increase. The HOMO-1 of dyes D1/TiO$_2$-D4/TiO$_2$, lying at about, −6.02, −5.89, −6.00, and −5.71 eV (see Table S1), which is about 1.03, 1.02, 1.02, and 1.03 eV below their respective HOMO. The HOMO and HOMO-1 levels of dyes D1–D4 are almost unchanged before and after binding on the TiO$_2$ surface. The LUMO levels (see Figure 9b) of dyes D1/TiO$_2$-D4/TiO$_2$ are −3.44, −3.43, −3.47, and −3.43 eV, respectively, indicating that the LUMO levels have no obvious change. The LUMO+1 levels of dyes D1/TiO$_2$-D4/TiO$_2$, lying at about −3.41, −3.40, −3.40, and −3.40 eV (see Table S1), there is no obvious change compared to their LUMO levels. Compared to the isolated dyes, the LUMO level of dyes/TiO$_2$ has no obvious change. The energy gaps of dyes D1/TiO$_2$–D4/TiO$_2$ are 1.55, 1.44, 1.51, and 1.25 eV, respectively. The energy gaps of dyes D2/TiO$_2$ and D4/TiO$_2$ are lower than that of A1/TiO$_2$ due to the higher HOMO energy level. Compared to their isolated dyes, the energy gap of dyes/TiO$_2$ has no obvious change. Molecular electrostatic potential (MEP) are shown in Figure 12. As shown in Figure 12, the most positive potential is found on carboxyl hydrogen atom, which is preferred area for

nucleophilic attack. While the greatest negative potential is observed on nitrogen atom of -CN group, which is the preferred site of electrophilic attack.
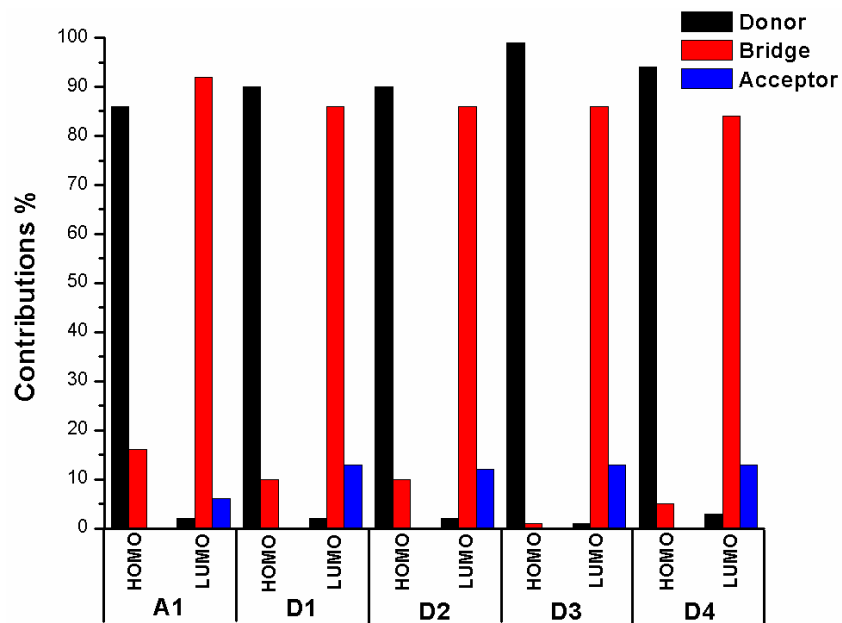

Figure 11. Molecular orbital compositions of the individual groups in HOMO and LUMO of D1–D4 and A1 in chloroform solvent.
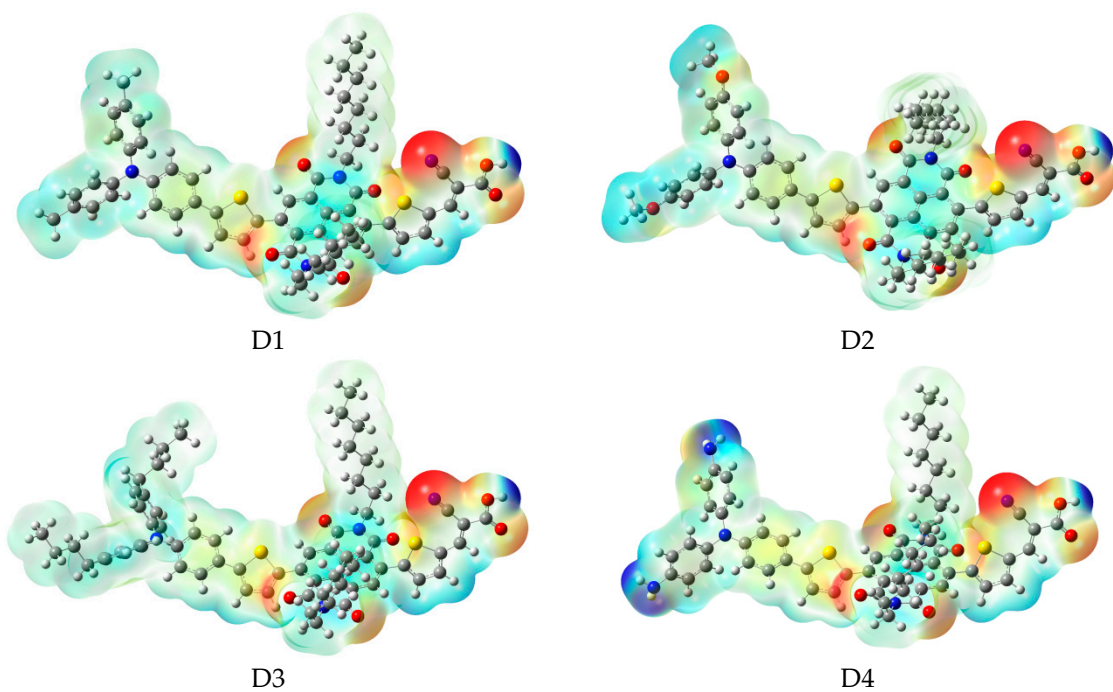

Figure 12. Molecular electrostatic potential plots of dyes D1–D4 in chloroform solvent.

The photophysical parameters of dyes D1–D4 are listed in Table 2, and the UV–vis absorption spectra are shown in Figure 13a. The first excited states of dyes D1–D4 show a transition from the HOMO to the LUMO. The maximum absorption peaks (λ_{max}) of dyes are in following order; D4 (571 nm) > D2 (548 nm) > D1 (534 nm) > D3 (532 nm), which exhibit 46, 23, 9, and 7 nm red shift compared to that of A1, respectively. After binding on the TiO$_2$ surface, the excited state properties

and absorption spectra are shown in Table 2 and Figure 13b. The maximum absorption peaks (λ_{max}) of dyes/TiO$_2$ are in following order; D4/TiO$_2$ (581 nm) > D2/TiO$_2$ (553 nm) > D1/TiO$_2$ (538 nm) = D3/TiO$_2$ (538 nm), which exhibit 52, 24, 9, and 9 nm red shift compared to that of A1/TiO$_2$, respectively. The first excited states of all the dye/TiO$_2$ show a major contribution from HOMO to LUMO. Compared to the isolated dyes, the maximum absorption peak (λ_{max}) is 4, 5, 6, and 10 nm red-shift for dyes D1/TiO$_2$–D4/TiO$_2$, respectively. As shown in Figure 14, the charge difference density (CDD) of D1/TiO$_2$–D4/TiO$_2$ has a similar electronic distribution compared to A1/TiO$_2$. It is worth mentioning that the density increment region of the excited state S3 for D4/TiO$_2$ is mainly distributed on acceptor and TiO$_2$, indicating that a better intramolecular charge transfer when the transition occurs compared to A1/TiO$_2$.

(a)

(b)
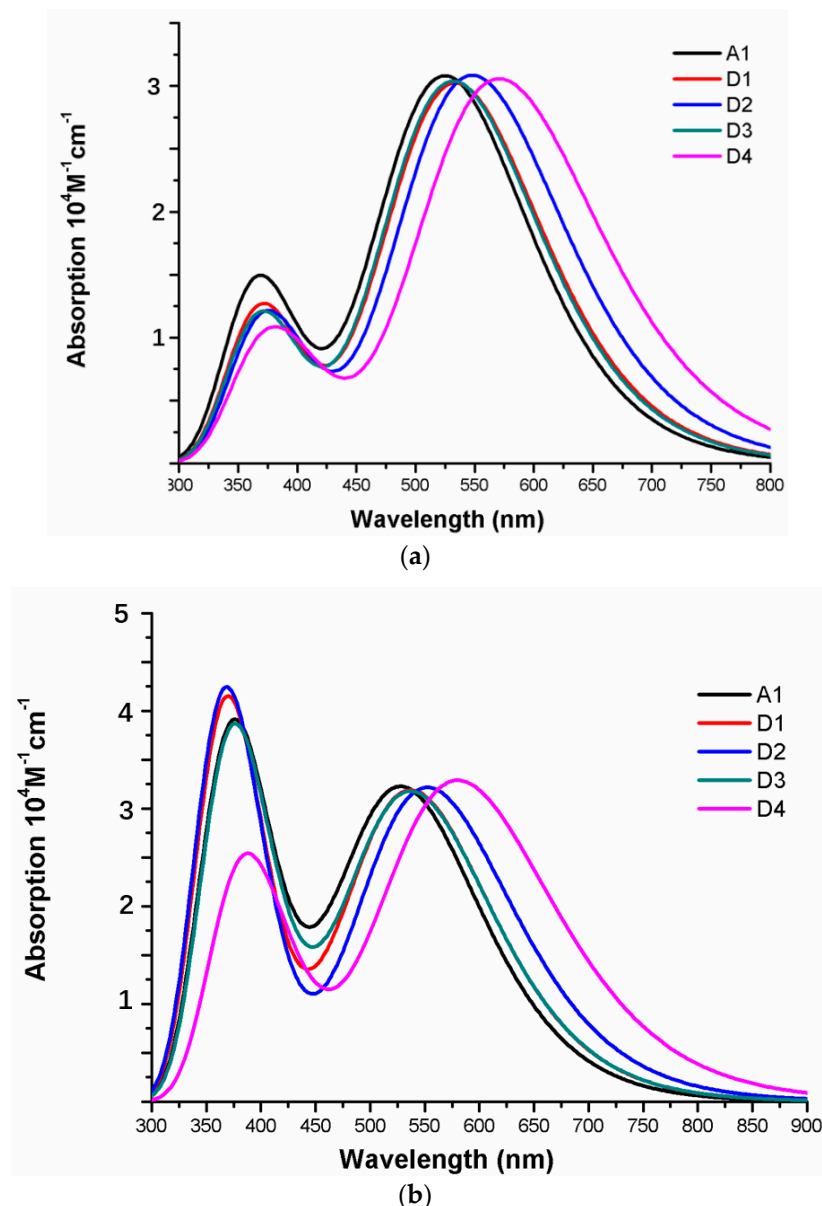
Figure 13. Absorption spectra of (**a**) isolated dyes D1–D4 and A1, (**b**) dyes D1–D4 and A1 after bound to TiO$_2$ surface in chloroform solvent.
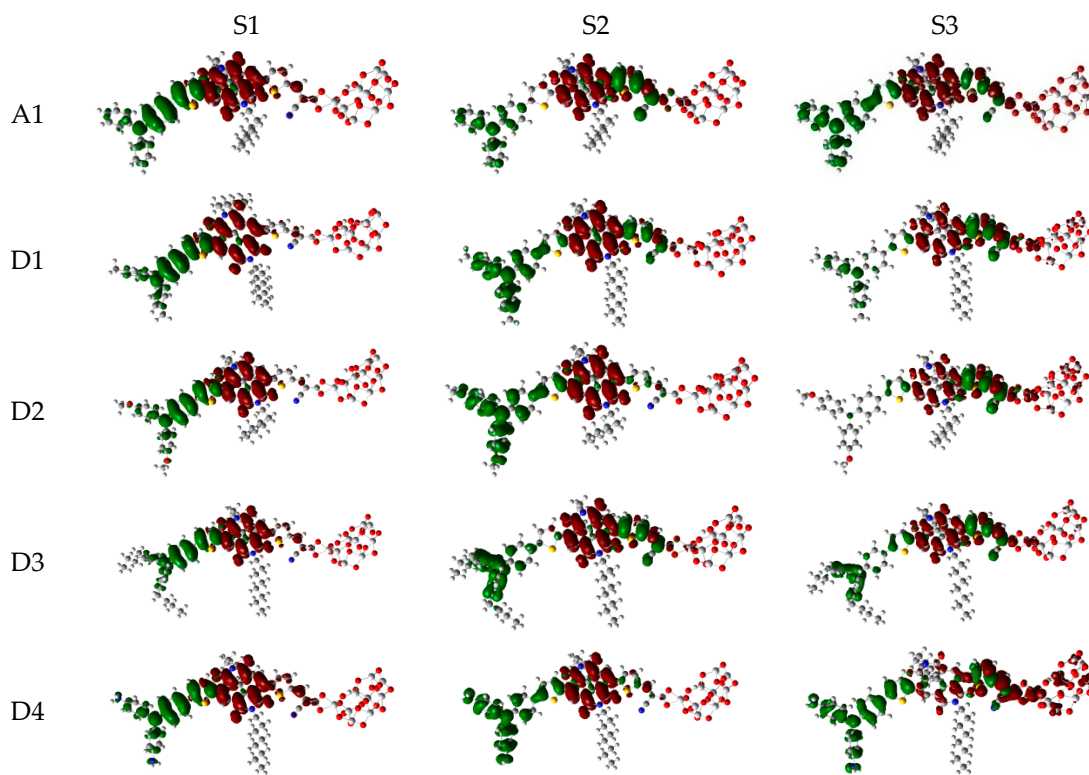
Figure 14. Charge difference density (CDD) of the selected excited state for dyes D1–D4 and A1 after bound to TiO_2 surface in chloroform solvent.

As shown in Table 3, the maximum emission wavelengths (λ_{em}) of dyes exhibit higher wavelengths (~150 nm) than their maximum absorption wavelengths (λ_{max}). D4 has largest λ_{em} at 723 nm which is 152 nm higher than its λ_{max}. D2 exhibit λ_{em} with 697 nm, which is 149 nm higher than its λ_{max}. While D1 and D3 have lowest λ_{em} with 685 nm, which is 151 and 153 nm higher than its λ_{max}. All dyes exhibit same electronic transition from HOMO to LUMO. Compared to A1, the maximum emission wavelength of D1–D4 show red shift by 9, 21, 9, and 47 nm, respectively.

The oscillator strength (f) is an important factor affecting the light harvesting efficiency (LHE). As shown in Table 4, the oscillator strengths (f) of D1–D4 are in the range of 0.7459-0.7609, which have no obvious change compared to A1 (0.7597). Hence light harvesting efficiency (LHE) of D1–D4 has no obvious change, and the values are 0.820, 0.827, 0.822, and 0.824, respectively. The calculated driving force of electron injection (ΔG^{inject}) are in following order; D1 > D3 > D2 > D4, which are more negative than that of A1, suggesting that dyes D1–D4 will exhibit faster electron injection and larger short-circuit photocurrent (J_{SC}). The reorganization energy (ΔG_{reg}) of dyes D1–D4 are 0.38, 0.27, 0.38, and 0.08 eV, respectively, which are lower than A1 (0.48 eV). Hence dyes P1–P6 will have higher power conversion efficiency due to the lower reorganization energy (ΔG_{reg}). The eV_{OC} values of D1–D4 are in the range of 0.58 to 0.63 eV, which have no obvious change compared to A1 (0.57 eV).

After binding on the TiO_2 surface, the oscillator strengths (f) of $D1/TiO_2$-$D4/TiO_2$ are in the range of 0.7819-0.8108, which have no obvious change compared to A1 (0.7923). The light harvesting efficiency (LHE) of $D1/TiO_2$-$D4/TiO_2$ are 0.836, 0.839, 0.835, and 0.845, respectively. There is no obvious change compared to $A1/TiO_2$ (0.839). The driving force of electron injection (ΔG^{inject}) of $D1/TiO_2$–$D4/TiO_2$ are more negative than that of $A1/TiO_2$, $D2/TiO_2$ exhibit most negative ΔG^{inject} (−2.51 eV). The eV_{OC} values of $D1/TiO_2$–$D4/TiO_2$ have no obvious change compared to $A1/TiO_2$. $D4/TiO_2$ has lowest ΔG_{reg}, followed by $D2/TiO_2$, $D3/TiO_2$, and $D1/TiO_2$. Compared to the isolated dyes, the driving force of electron injection (ΔG^{inject}) of $D1/TiO_2$ and $D2/TiO_2$ increases slightly, while $D3/TiO_2$ and

D4/TiO$_2$ have no obvious change. The light harvesting efficiency (LHE), reorganization energy (ΔG_{reg}) and eV_{OC} of D1–D4 have no obvious change before and after binding on the TiO$_2$ surface.

4. Conclusions

In this work, we have systematically investigated optical and electrical properties of D-π-A type dyes designed by introducing different functional groups on the donor and π-spacer. The results indicate that π-spacer in P1–P6 exhibit rigid structures, which will enhance electrons more easily transferred from donor to acceptor. P1 and P3–P6 show red shift compared to A1. In particular, light harvesting efficiency (LHE), driving force of electron injection (ΔG^{inject}), reorganization energy (ΔG_{reg}), and eV_{OC} of P1–P6 which related to the short-circuit current density (J_{SC}) and open-circuit photovoltage (V_{OC}), are superior to those of A1. Therefore, P1–P6 are regarded as outstanding candidates for use in DSSCs. Furthermore, the donor group in D2 and D4 exhibit lower energy gap and great red shift compared to A1. D4 shows the more driving force of electron injection (ΔG^{inject}) and lower reorganization energy (ΔG_{reg}) among the D1–D4, which are superior to those of A1. This is beneficial to improving the short-circuit current density (J_{SC}). Above all, P1–P6 and D4 are promising organic dyes and display better photoelectric performance in rational molecular engineering of sensitizers combining high photovoltaic efficiency.

References

1. O'Regan, B.; Grätzel, M. A Low-Cost High-Efficiency Solar Cell Based on Dye-Sensitized Colloidal TiO$_2$ Films. *Nature* **1991**, *353*, 737–740. [CrossRef]
2. Duncan, W.R.; Prezhdo, O.V. Theoretical studies of photoinduced electron transfer in dye-sensitized TiO(2). *Annu. Rev. Phys. Chem.* **2007**, *58*, 143–184. [CrossRef]
3. Gratzel, M. Photoelectrochemical cells. *Nature* **2001**, *414*, 338–344. [CrossRef] [PubMed]
4. Gong, J.W.; Sumathy, K.; Qian, Q.Q.; Zhou, Z.P. Review on dye-sensitized solar cells (DSSCs): Advanced techniques and research trends. *Renew. Sustain. Energy Rev.* **2017**, *68*, 234–246. [CrossRef]
5. Gendron, D.; Leclerc, M. New conjugated polymers for plastic solar cells. *Energy Environ. Sci.* **2011**, *4*, 1225–1237. [CrossRef]
6. Perera, I.R.; Daeneke, T.; Makuta, S.; Yu, Z.; Tachibana, Y.; Mishra, A.; Bäuerle, P.; Ohlin, C.A.; Bach, U.; Spiccia, L. Application of the Tris(acetylacetonato)iron(III)/(II) Redox Couple in p-Type Dye-Sensitized Solar Cells. *Angew. Chem. Int. Ed.* **2015**, *54*, 3758–3762. [CrossRef]
7. Long, R.; Prezhdo, O.V. Ab Initio Nonadiabatic Molecular Dynamics of the Ultrafast Electron Injection from a PbSe Quantum Dot into the TiO$_2$ Surface. *J. Am. Chem. Soc.* **2011**, *133*, 19240–19249. [CrossRef]
8. Wang, J.G.; Li, W.H.; Xu, X.F.; Ma, F.C.; Sun, M.T. Plasmon-Exciton Coupling Interaction for Surface Catalytic Reactions. *Chem. Rec.* **2018**, *18*, 481–490. [CrossRef]
9. Nazeeruddin, M.K.; Péchy, P.; Renouard, T.; Zakeeruddin, S.M.; Humphry-Baker, R.; Comte, P.; Liska, P.; Cevey, L.; Costa, E.; Shklover, V.; et al. Engineering of Efficient Panchromatic Sensitizers for Nanocrystalline TiO2-Based Solar Cells. *J. Am. Chem. Soc.* **2001**, *123*, 1613–1624. [CrossRef]

10. Mathew, S.; Yella, A.; Gao, P.; Humphry-Baker, R.; CurchodBasile, F.E.; Ashari-Astani, N.; Tavernelli, I.; Rothlisberger, U.; NazeeruddinMd, K.; Grätzel, M. Dye-sensitized solar cells with 13% efficiency achieved through the molecular engineering of porphyrin sensitizers. *Nat. Chem.* **2014**, *6*, 242–247. [CrossRef]

11. Kim, S.H.; Kim, H.W.; Sakong, C.; Namgoong, J.; Park, S.W.; Ko, M.J.; Lee, C.H.; Lee, W.I.; Kim, J.P. Effect of five-membered heteroaromatic linkers to the performance of phenothiazine-based dye-sensitized solar cells. *Org. Lett.* **2011**, *13*, 5784–5787. [CrossRef] [PubMed]

12. Tseng, C.-Y.; Taufany, F.; Nachimuthu, S.; Jiang, J.-C.; Liaw, D.-J. Design strategies of metal free-organic sensitizers for dye sensitized solar cells: Role of donor and acceptor monomers. *Org. Electron.* **2014**, *15*, 1205–1214. [CrossRef]

13. Vollbrecht, J.; Bock, H.; Wiebeler, C.; Schumacher, S.; Kitzerow, H. Polycyclic Aromatic Hydrocarbons Obtained by Lateral Core Extension of Mesogenic Perylenes: Absorption and Optoelectronic Properties. *Chem. A Eur. J.* **2014**, *20*, 12026–12031. [CrossRef] [PubMed]

14. Feng, J.; Jiao, Y.; Ma, W.; Nazeeruddin, M.K.; Grätzel, M.; Meng, S. First principles design of dye molecules with ullazine donor for dye sensitized solar cells. *J. Phys. Chem. C* **2013**, *117*, 3772–3778. [CrossRef]

15. Santhanamoorthi, N.; Lo, C.-M.; Jiang, J.-C. Molecular design of porphyrins for dye-sensitized solar cells: a DFT/TDDFT study. *J. Phys. Chem. Lett.* **2013**, *4*, 524–530. [CrossRef]

16. Bellier, Q.; Pégaz, S.; Aronica, C.; Guennic, B.L.; Andraud, C.; Maury, O. Near-infrared nitrofluorene substitued aza-boron-dipyrromethenes dyes. *Org. Lett.* **2011**, *13*, 22–25. [CrossRef] [PubMed]

17. Yin, Y.; Miao, P.; Zhang, Y.; Han, J.; Zhang, X.; Gong, Y.; Gu, L.; Xu, C.; Yao, T.; Xu, P.; et al. Significantly Increased Raman Enhancement on MoX2 (X = S, Se) Monolayers upon Phase Transition. *Adv. Funct. Mater.* **2017**, *27*, 1606694. [CrossRef]

18. Xu, B.; Li, Y.; Song, P.; Ma, F.; Sun, M. Photoactive layer based on T-shaped benzimidazole dyes used for solar cell: from photoelectric properties to molecular design. *Sci. Rep.* **2017**, *7*, 45688. [CrossRef]

19. Katono, M.; Wielopolski, M.; Marszalek, M.; Bessho, T.; Moser, J.-E.; Humphry-Baker, R.; Zakeeruddin, S.M.; Grätzel, M.J. Effect of Extended π-Conjugation of the Donor Structure of Organic D–A– π–A Dyes on the Photovoltaic Performance of Dye-Sensitized Solar Cells. *J. Phys. Chem. C* **2014**, *118*, 16486–16493. [CrossRef]

20. Paramasivam, M.; Gupta, A.; Raynor, A.M.; Bhosale, S.V.; Bhanuprakash, K.; Rao, V.J. Small band gap D-π-A-π-D benzothiadiazole derivatives with low-lying HOMO levels as potential donors for applications in organic photovoltaics: a combined experimental and theoretical investigation. *RSC Adv.* **2014**, *4*, 35318–35331. [CrossRef]

21. Namuangruk, S.; Fukuda, R.; Ehara, M.; Meeprasert, J.; Khanasa, T.; Morada, S.; Kaewin, T.; Jungsuttiwong, S.; Sudyoadsuk, T.; Promarak, V.J. D–D–π–A-Type Organic Dyes for Dye-Sensitized Solar Cells with a Potential for Direct Electron Injection and a High Extinction Coefficient: Synthesis, Characterization, and Theoretical Investigation. *J. Phys. Chem. C* **2012**, *116*, 25653–25663. [CrossRef]

22. Xie, M.; Wang, J.; Bai, F.-Q.; Hao, L.; Zhang, H.-X. Discovering the intermediate of dye regeneration in dye-sensitized solar cells: Theoretical investigations on the interaction between organic dye with different donors and X−/X3− (X = I, Br). *Dyes Pigment.* **2015**, *120*, 74–84. [CrossRef]

23. Li, Y.; Xu, B.; Song, P.; Ma, F.; Sun, M.J. D–A– π–A system: Light harvesting, charge transfer, and molecular designing. *J. Phys. Chem. C.* **2017**, *121*, 12546–12561. [CrossRef]

24. Li, Y.; Qi, D.; Song, P.; Ma, F. Fullerene-based photoactive layers for heterojunction solar cells: Structure, absorption spectra and charge transfer process. *Materials* **2015**, *8*, 42–56. [CrossRef]

25. Haid, S.; Marszalek, M.; Mishra, A.; Wielopolski, M.; Teuscher, J.; Moser, J.-E.; Humphry-Baker, R.; Zakeeruddin, S.M.; Grätzel, M.; Bäuerle, P. Significant Improvement of Dye-Sensitized Solar Cell Performance by Small Structural Modification in π-Conjugated Donor–Acceptor Dyes. *Adv. Funct. Mater.* **2012**, *22*, 1291–1302. [CrossRef]

26. Mai, C.-L.; Huang, W.-K.; Lu, H.-P.; Lee, C.-W.; Chiu, C.-L.; Liang, Y.-R.; Diau, E.W.-G.; Yeh, C.-Y. Synthesis and characterization of diporphyrin sensitizers for dye-sensitized solar cells. *Chem. Commun.* **2010**, *46*, 809–811. [CrossRef]

27. Imahori, H.; Matsubara, Y.; Iijima, H.; Umeyama, T.; Matano, Y.; Ito, S.; Niemi, M.; Tkachenko, N.V.; Lemmetyinen, H. Effects of meso-Diarylamino Group of Porphyrins as Sensitizers in Dye-Sensitized Solar Cells on Optical, Electrochemical, and Photovoltaic Properties. *J. Phys. Chem. C* **2010**, *114*, 10656–10665. [CrossRef]

28. Han, L.; Wu, H.; Cui, Y.; Zu, X.; Ye, Q.; Gao, J. Synthesis and density functional theory study of novel coumarin-type dyes for dye sensitized solar cells. *J. Photochem. Photobiol. A Chem.* **2014**, *290*, 54–62. [CrossRef]

29. Seo, K.D.; Song, H.M.; Lee, M.J.; Pastore, M.; Anselmi, C.; de Angelis, F.; Nazeeruddin, M.K.; Gräetzel, M.; Kim, H.K. Coumarin dyes-containing low-band-gap chromophores for dye-sensitised solar cells. *Dyes Pigment.* **2011**, *90*, 304–310. [CrossRef]

30. Tarsang, R.; Promarak, V.; Sudyoadsuk, T.; Namuangruk, S.; Jungsuttiwong, S. Tuning the electron donating ability in the triphenylamine-based D-π-A architecture for highly efficient dye-sensitized solar cells. *J. Photochem. Photobiol. A Chem.* **2014**, *273*, 8–16. [CrossRef]

31. Wu, F.; Zhao, S.; Lee, L.T.L.; Wang, M.; Chen, T.; Zhu, L. Novel D-π-A organic sensitizers containing diarylmethylene-bridged triphenylamine and different spacers for solar cell application. *Tetrahedron Lett.* **2015**, *56*, 1233–1238. [CrossRef]

32. Patil, D.; Jadhav, M.; Avhad, K.; Chowdhury, T.H.; Islam, A.; Bedjac, I.; Sekar, N. A new class of triphenylamine based novel sensitizers for DSSC: A comparative study of three different anchoring groups. *New J. Chem.* **2018**, *42*, 11555–11564. [CrossRef]

33. Rudolph, M.; Yoshida, T.; Miura, H.; Schlettwein, D. Improvement of light harvesting by addition of a long-wavelength absorber in dye-sensitized solar cells based on ZnO and indoline dyes. *J. Phys. Chem. C* **2015**, *119*, 1298–1311. [CrossRef]

34. Cai, N.; Moon, S.-J.; Cevey-Ha, L.; Moehl, T.; Humphry-Baker, R.; Wang, P.; Zakeeruddin, S.M.; Grätzel, M. An organic D-π-A dye for record efficiency solid-state sensitized heterojunction solar cells. *Nano Lett.* **2011**, *11*, 1452–1456. [CrossRef]

35. Xu, M.; Li, R.; Pootrakulchote, N.; Shi, D.; Guo, J.; Yi, Z.; Zakeeruddin, S.M.; Grätzel, M.; Wang, P. Energy-level and molecular engineering of organic D-π-A sensitizers in dye-sensitized solar cells. *J. Phys. Chem. C* **2008**, *112*, 19770–19776. [CrossRef]

36. Liang, M.; Chen, J. Arylamine organic dyes for dye-sensitized solar cells. *Chem. Soc. Rev.* **2013**, *42*, 3453–3488. [CrossRef]

37. Urbani, M.; Grätzel, M.; Nazeeruddin, M.K.; Torres, T. Meso-substituted porphyrins for dye-sensitized solar cells. *Chem. Rev.* **2014**, *114*, 12330–12396. [CrossRef]

38. Mishra, A.; Fischer, M.K.R.; Bäuerle, P. Metal-free organic dyes for dye-sensitized solar cells: From structure: Property relationships to design rules. *Angew. Chem. Int. Ed.* **2009**, *48*, 2474–2499. [CrossRef]

39. Song, P.; Zhou, Q.; Li, Y.Z.; Ma, F.C.; Sun, M.T. Vibronic quantized tunneling controlled photoinduced electron transfer in an organic solar cell subjected to an external electric field. *Phys. Chem. Chem. Phys.* **2017**, *19*, 16105–16112. [CrossRef]

40. Kim, S.; Lee, J.K.; Kang, S.O.; Ko, J.; Yum, J.H.; Fantacci, S.; de Angelis, F.; di Censo, D.; Nazeeruddin, M.K.; Grätzel, M. Molecular engineering of organic sensitizers for solar cell applications. *J. Am. Chem. Soc.* **2006**, *128*, 16701–16707. [CrossRef]

41. Chen, C.; Yang, X.; Cheng, M.; Zhang, F.; Zhao, J.; Sun, L. A draft sequence for the genome of the domesticated silkworm (Bombyx mori). *ACS Appl. Mater. Interfaces* **2013**, *5*, 10960–10965. [CrossRef]

42. Kim, K.-M.; Hong, J.-I. Design of high-performance dye-sensitized solar cells by variation of the dihedral angles of dyes. *Tetrahedron* **2016**, *72*, 8387–8392. [CrossRef]

43. Panneerselvam, M.; Kathiravan, A.; Solomon, R.V.; Jaccob, M. The role of π-linkers in tuning the optoelectronic properties of triphenylamine derivatives for solar cell applications–A DFT/TDDFT study. *Phys. Chem. Chem. Phys.* **2017**, *19*, 6153–6163. [CrossRef]

44. Biswas, A.K.; Das, A.; Ganguly, B. Can fused-pyrrole rings act as better π-spacer units than fused-thiophene in dye-sensitized solar cells? A computational study. *New J. Chem.* **2016**, *40*, 9304–9312. [CrossRef]

45. Bobe, S.R.; Gupta, A.; Rananaware, A.; Bilic, A.; Xiang, W.; Li, J.; Bhosale, S.V.; Bhosale, S.V.; Evans, R.A. Insertion of a naphthalenediimide unit in a metal-free donor–acceptor organic sensitizer for efficiency enhancement of a dye-sensitized solar cell. *Dyes Pigment.* **2016**, *134*, 83–90. [CrossRef]

46. Narayan, M.R. Dye sensitized solar cells based on natural photosensitizers. *Renew. Sustain. Energy Rev.* **2012**, *16*, 208–215. [CrossRef]

47. Zhang, J.; Li, H.-B.; Sun, S.-L.; Geng, Y.; Wu, Y.; Su, Z.-M. Density functional theory characterization and design of high-performance diarylamine-fluorene dyes with different π spacers for dye-sensitized solar cells. *J. Mater. Chem.* **2012**, *22*, 568–576. [CrossRef]

48. Preat, J.; Jacquemin, D.; Michaux, C.; Perpète, E.A. Improvement of the efficiency of thiophene-bridged compounds for dye-sensitized solar cells. *Chem. Phys.* **2010**, *376*, 56–68. [CrossRef]

49. Zhang, J.; Kan, Y.-H.; Li, H.-B.; Geng, Y.; Wu, Y.; Su, Z.-M. How to design proper π-spacer order of the D-π-A dyes for DSSCs? A density functional response. *Dyes Pigment.* **2012**, *95*, 313–321. [CrossRef]

50. Marinado, T.; Nonomura, K.; Nissfolk, J.; Karlsson, M.K.; Hagberg, D.P.; Sun, L.; Mori, S.; Hagfeldt, A. How the nature of triphenylamine-polyene dyes in dye-sensitized solar cells affects the open-circuit voltage and electron lifetimes. *Langmuir* **2010**, *26*, 2592–2598. [CrossRef]

51. Rühle, S.; Greenshtein, M.; Chen, S.G.; Merson, A.; Pizem, H.; Sukenik, C.S.; Cahen, D.; Zaban, A. Molecular adjustment of the electronic properties of nanoporous electrodes in dye-sensitized solar cells. *J. Phys. Chem. B* **2005**, *109*, 18907–18913. [CrossRef] [PubMed]

52. Ditchfield, R.; Hehre, W.J.; Pople, J.A. Self-consistent molecular-orbital methods. IX. An extended Gaussian-type basis for molecular-orbital studies of organic molecules. *J. Chem. Phys.* **1971**, *54*, 724–728.

53. Miehlich, B.; Savin, A.; Stoll, H.; Preuss, H. Results obtained with the correlation energy density functionals of Becke and Lee, Yang and Parr. *Chem. Phys. Lett.* **1989**, *157*, 200–206. [CrossRef]

54. Stratmann, R.E.; Scuseria, G.E.; Frisch, M.J. An efficient implementation of time-dependent density-functional theory for the calculation of excitation energies of large molecules. *J. Chem. Phys.* **1998**, *109*, 8218–8224. [CrossRef]

55. Yanai, T.; Tew, D.P.; Handy, N.C. A new hybrid exchange–correlation functional using the Coulomb-attenuating method (CAM-B3LYP). *Chem. Phys. Lett.* **2004**, *393*, 51–57. [CrossRef]

56. Ding, W.-L.; Wang, D.-M.; Geng, Z.-Y.; Zhao, X.-L.; Yan, Y.-F. Molecular engineering of indoline-based D–A−π–A organic sensitizers toward high efficiency performance from first-principles calculations. *J. Phys. Chem. C* **2013**, *117*, 17382–17398. [CrossRef]

57. Kathiravan, A.; Srinivasan, V.; Khamrang, T.; Velusamy, M.; Jaccob, M.; Pavithra, N.; Anandan, S.; Velappan, K. Pyrene based D–π–A architectures: synthesis, density functional theory, photophysics and electron transfer dynamics. *Phys. Chem. Chem. Phys.* **2017**, *19*, 3125–3135. [CrossRef] [PubMed]

58. Chaitanya, K.; Ju, X.-H.; Heron, B.M. Theoretical study on the light harvesting efficiency of zinc porphyrin sensitizers for DSSCs. *Rsc Adv.* **2014**, *4*, 26621–26634. [CrossRef]

59. Dong, C.K.; Xiang, W.C.; Huang, F.Z.; Fu, D.C.; Huang, W.C.; Bach, U.; Cheng, Y.B.; Li, X.; Spiccia, L. Controlling Interfacial Recombination in Aqueous Dye-Sensitized Solar Cells by Octadecyltrichlorosilane Surface Treatment. *Angew. Chem. Int. Ed.* **2014**, *53*, 6933–6937. [CrossRef]

60. Frisch, M.J.; Trucks, G.W.; Schlegel, H.B.; Scuseria, G.E.; Robb, M.A.; Cheeseman, J.R.; Scalmani, G.; Barone, V.; Petersson, G.A.; Nakatsuji, H.; et al. *Gaussian 09, Revision A.01, Gaussian*; Wallingford's Inc.: Oakland, CA, USA, 2009.

61. Jin, J.-L.; Li, H.-B.; Geng, Y.; Wu, Y.; Duan, Y.-A.; Su, Z.-M. Theoretical Insight into the Origin of Large Stokes Shift and Photophysical Properties of Anilido-Pyridine Boron Difluoride Dyes. *ChemPhysChem* **2012**, *13*, 3714–3722. [CrossRef]

62. Gajalakshmi, D.; Solomon, R.V.; Tamilmani, V.; Boobalan, M.; Venuvanalingam, P. A DFT/TDDFT mission to probe push–pull vinyl coupled thiophene oligomers for optoelectronic applications. *RSC Adv.* **2015**, *5*, 50353–50364. [CrossRef]

63. Jungsuttiwong, S.; Tarsang, R.; Sudyoadsuk, T.; Promarak, V.; Khongpracha, P.; Namuangruk, S. Theoretical study on novel double donor-based dyes used in high efficient dye-sensitized solar cells: the application of TDDFT study to the electron injection process. *Org. Electron.* **2013**, *14*, 711–722. [CrossRef]

64. Liu, Q.; Lin, X.C.; Mi, L.; Gao, N.; Song, P.; Ma, F.C.; Li, Y.Z. Characterizations of Efficient Charge Transfer and Photoelectric Performance in the Cosensitization of Solar Cells. *Appl. Sci.* **2018**, *8*, 1122. [CrossRef]

65. Daeneke, T.; Mozer, A.J.; Uemura, Y.; Makuta, S.; Fekete, M.; Tachibana, Y.; Koumura, N.; Bach, U.; Spiccia, L. Dye regeneration kinetics in dye-sensitized solar cells. *J. Am. Chem. Soc.* **2012**, *134*, 16925–16928. [CrossRef] [PubMed]

66. Li, M.; Kou, L.; Diao, L.; Zhang, Q.; Li, Z.; Wu, Q.; Lu, W.; Pan, D.; Wei, Z. Theoretical study of WS-9-Based organic sensitizers for unusual vis/NIR absorption and highly efficient dye-sensitized solar cells. *J. Phys. Chem. C* **2015**, *119*, 9782–9790. [CrossRef]

67. Zhang, C.-R.; Liu, Z.-J.; Chen, Y.-H.; Chen, H.-S.; Wu, Y.-Z.; Feng, W.; Wang, D.-B. DFT and TD-DFT study on structure and properties of organic dye sensitizer TA-St-CA. *Curr. Appl. Phys.* **2010**, *10*, 77–83. [CrossRef]

68. Dong, C.K.; Li, X.; Jin, P.F.; Zhao, W.; Chu, J.; Qi, J.Y. Intersubunit Electron Transfer (IET) in Quantum Dots/Graphene Complex: What Features Does IET Endow the Complex with? *J. Phys. Chem. C* **2012**, *116*, 15833–15838. [CrossRef]

69. Eriksson, S.K.; Josefsson, I.; Ellis, H.; Amat, A.; Pastore, M.; Oscarsson, J.; Lindblad, R.; Eriksson, A.I.K.; Johansson, E.M.J.; Boschloo, G.; et al. Geometrical and energetical structural changes in organic dyes for dye-sensitized solar cells probed using photoelectron spectroscopy and DFT. *Phys. Chem. Chem. Phys.* **2016**, *18*, 252–260. [CrossRef]